Università degli Studi di Ferrara

DOTTORATO DI RICERCA IN
SCIENZE DELL'INGEGNERIA

CICLO XXIII

COORDINATORE Prof. Trillo Stefano

ON THE TRIBOLOGICAL BEHAVIOUR OF METAL/CERAMIC AND METAL/METAL COUPLINGS

Settore Scientifico Disciplinare ING-IND/21

Dottorando
Dott. Soffritti Chiara

_____
(firma)

Tutore
Prof. Garagnani Gian Luca

_____
(firma)

Anni 2008/2010

To my husband and my sons

PREFACE

The research activity that I carried out during my PhD is the result of three years' full-time study at the University of Ferrara, Italy, from January 2008 to December 2010. The research and experimental work were performed at the Engineering Department of the University of Ferrara (ENDIF), with Professor Gian Luca Garagnani being my main supervisor.

During my PhD, I focused on the study of the tribological behaviour of metal/ceramic and metal/metal couplings. The results were published or submitted for publication in national conference proceedings, as well as in national journals, throughout the three years of my PhD. Most of my work is here presented as a collection of three articles. The papers included in this thesis are reported in the same format they were published or in a preprint version. Each paper is an individual piece of work with separate sections including: abstract, introduction, materials and experimental details, results and discussion, conclusions and references. The introduction of this thesis is intended to provide a summary of the main aims of the articles and the principal conclusions obtained.

Moreover, during my PhD I analysed the main properties of different alloys. The other research work and publications, developed during the period of my doctoral studies but not explicitly included in this thesis, are reported below:

a. COPPER ALLOYS

Microstructural characterisations were performed on a bronze monument located at Certosa in Ferrara, which was built in Roberto Fabbri's memory. The research was carried out as part of *"Progetto di Gestione del Patrimonio Culturale Locale"*. The research activity confirmed that the most common analytical methods, typical of metallographic investigations, can be successfully applied to the metallic materials of archaeological interest in order to identify the alloy and study the production and processing technologies. Instruments for metallographic analysis were also used to understand the main corrosion mechanisms and to define the restoration work needed to improve the preservation of local artistic heritage. The results of this research project were published in:

G. L. GARAGNANI, C. SOFFRITTI, F. ZANOTTO, F. ZUCCHI, *"**Analisi chimiche e microstrutturali sulla statua in bronzo del monumento funerario a Roberto Fabbri (Certosa di Ferrara, 1914)**"*, Competenze e strumenti per il patrimonio culturale. il caso del territorio ferrarese, cured by R. Dalla Negra, F. Donato, G. L. Garagnani, B. Sala, R. Varese, Corbo Ed., Ferrara, (2010), pp 135-147.

In another activity, the microstructural characterization of ancient coins belonging to *Tesoretto di Alberone* (XV-XVI century) was carried out. In particular, Scanning Electron Microscope (SEM) equipped with an EDS microprobe was used to evaluate the chemical composition of the alloy and to identify macro and micro-segregations and non-metallic inclusions. Moreover, X-ray diffraction (XRD) tests were subsequently performed in order to confirm SEM analyses. Vickers microhardness measurements and optical microscope observations were also carried out to correlate the microstructure to the production technologies normally used during the Renaissance. The results were published in:

C. SOFFRITTI, S. PEPI, G. L. GARAGNANI, C. VACCARO, M. T. GULINELLI, *"**Caratterizzazione microstrutturale di serie monetali appartenenti al Tesoretto di Alberone (sec. XV-XVI)**"*, Presented at Convegno A.I.A.r. 2011, *"La Scienza per l'Arte Contemporanea"*, Ferrara, Italy, 1-4 March 2011.

b. Ni-Ti ALLOYS

Ni-Ti shape memory alloys (SMAs) show attractive functional properties for a number of engineering and medical applications. These alloys have the potential to be used in the design of actuators, sensors and, especially, functional structures, in which they are directly or indirectly embedded in a polymer matrix. An initial research activity involved the realisation of a functional structure in which NiTi wires were embedded in a Nylon 66 thermoplastic resin. The wires were previously characterized by tensile tests in both martensitic and austenitic phases, to evaluate elastic moduli, plateau stresses and the maximum recoverable strain due to the shape memory effect. The transformation temperatures were determined by Differential Scanning Calorimetry (DSC). The efficiency of stress and deformation transfer depends greatly on the interface strength between the wires and the surrounding matrix. Therefore, in another activity I focused on the evaluation of the interface strength between

NiTi wires and two kinds of thermosetting resins: polyester and vinylester. Different surface treatments were performed on the SMA wires in order to increase the performance of the wire-resin interface adhesion. In particular, chemical passivation by using acid solution and functionalization by using a silane coupling agent, were considered. Pull-out tests were carried out to quantify the improvement of the interface adhesion. Part of this research was presented at a national congress and another part was written in a preprint version:

M. MERLIN, C. SOFFRITTI, G. L. GARAGNANI, *"**Sviluppo di un composito funzionale a matrice termoplastica con fili in lega NiTi**"*, Proceedings of 33° Convegno Nazionale AIM, Brescia, Italy, 10-12 November 2010.

M. MERLIN, M. SCOPONI, C. SOFFRITTI, "***On the improved adhesion of NiTi wires embedded in polyester and vinylester resins***", preprint, 2011.

In addition, another important role of my PhD was to supervise the following theses, performed at the Engineering Department of the University of Ferrara:

1. Martina Berti (2008), "**Caratterizzazione dell'interfaccia tra fili NiTi e resine termoindurenti poliestere insatura e vinilestere**", Supervisors: G.L. Garagnani, M. Merlin, C. Soffritti.
2. Daniele Casari (2008), "**Analisi microstrutturale e comportamento a fatica di un acciaio HSLA al Nb-V**", Supervisors: G.L. Garagnani, M. Merlin, C. Soffritti.
3. Matteo Zuffi (VO), "**Studio delle caratteristiche microstrutturali e delle proprietà ad impatto dell'acciaio duplex SAF 2205 saldato mediante tecnologia SAW**", Supervisors: G.L. Garagnani, M. Merlin, C. Soffritti.
4. Stefano Succi (2008), "**Caratterizzazione microstrutturale e meccanica di getti motociclistici in lega A356-T6 realizzati con anima piena ed anima cava**", Supervisors: G.L. Garagnani, M. Merlin, C. Soffritti.
5. Andrea Artioli (2009), "**Analisi microstrutturale di un acciaio da cementazione sottoposto a prove d'usura**", Supervisors: G.L. Garagnani, C. Soffritti, R. Vazquez.
6. Valentina Boccia (2009), "**Valutazione del comportamento tribologico di riporti termici in Cr_2O_3 e Al_2O_3-13%TiO_2 ottenuti mediante spruzzatura al plasma**", Supervisors: G.L. Garagnani, C. Soffritti, R. Vazquez.

7. Anna Guerzoni (2010), "**Caratterizzazione tribologica delle punterie idrauliche di motori diesel dopo 1000 ore di funzionamento**", Supervisors: G.L. Garagnani, C. Soffritti.
8. Marco Vitali (2010), "**Comportamento ad usura di rivestimenti ceramici realizzati mediante spruzzatura termica**", Supervisors: G.L.Garagnani, C. Soffritti, R. Vazquez.
9. Marcello Bertasi (2010), "**Caratterizzazione microstrutturale di rivestimenti in Al_2O_3-13%TiO_2 e Cr_2O_3 ottenuti mediante APS (Air-Plasma-Spray)**", Supervisors: G.L. Garagnani, C. Soffritti, R. Vazquez.
10. Matteo Cisotto (2010), "**Caratterizzazione metallografica del rivestimento WC-12Co ottenuto mediante HVOF (High Velocity Oxygen-Fuel)**", Supervisors: G.L. Garagnani, C. Soffritti, R. Vazquez.
11. Valentina Mazzanti (2010), "**Valutazione del comportamento tribologico di riporti termici in WC-12Co e Cr3C2\37WC-18Me ottenuti con tecnologia HVOF**", Supervisors: G.L. Garagnani, C. Soffritti, M. Pinelli, C. Monticelli.
12. Andrea Covizzi (2010), "**Caratterizzazione metallografica del rivestimento WC-12Co ottenuto mediante APS (Atmospheric Plasma Spraying)**", Supervisors: G.L. Garagnani, C. Soffritti, R. Vazquez.
13. Salvatore Pepi (2010), "**Caratterizzazione petrografica e metallurgica di serie monetali appartenenti al tesoretto di Alberone (sec. XVI-XV)**", Supervisors: C. Vaccaro, G.L. Garagnani, C. Soffritti, M.T. Gulinelli.

Other publications:

M. MERLIN, C. SOFFRITTI, R. VAZQUEZ, V. MAZZANTI, G. L. GARAGNANI, *"**Analytical treatment of uncertainties for a macroscopic tribology instrumentation**"*, Accepted for presentation at 8th International Workshop on Progress in Analytical Chemistry & Materials Characterisation in the Steel and Metals Industries, CETAS, Luxembourg, 17-19 May 2011.

ACKNOWLEDGEMENTS

I would like to thank my supervisor Prof. Gian Luca Garagnani for proposing this PhD research project to me three years ago and for his advice, guidance and for sharing his expert knowledge with me.

I wish to thank all the people I have worked with during these three years of my PhD. In particular, I would like especially to thank Mattia for his invaluable advice, assistance and encouragement.

I would like to acknowledgement all my friends and my colleagues of Office 025: Monia, Agnese, Annalisa, Reyna, Fabio and Daniele.

Most of all I wish to thank my family. In particular, I would like to acknowledgement my husband Fadi for his great patience, love and understanding. A special thank to my beautiful son Elias for his love, brightness and joy of living that relieved even the most difficult days.

ABSTRACT

Corrosion, wear or the combined effects of these failure modes cost the industrial economies hundreds of billions of euros each year. One of the more effective ways to reduce damage due to corrosion and wear is to treat, or "engineer" the surface, so that it can perform functions that are distinct from those required by most materials. For example, steel is a very popular material, because it is inexpensive, strong and easily manufactured. Unfortunately, it is highly susceptible to corrosion in many environments and therefore needs to be coated in order to achieve a satisfactory life service. Small components can be painted, aluminized, electroplated, or clad with more corrosion resistant materials. For parts that also require wear strength, they can be thermally sprayed or coated with thin-films. Finally, when dealing with large components, the size, weight, and handling problems may limit the type of surface treatment to be considered. The aim of the research work presented in this PhD thesis was to study the interactions between the metal/ceramic and metal/metal coupling surfaces to improve the wear resistance of the materials in sliding motion. Most of my research work is included here as a collection of three papers submitted in the same format they were published or in a preprint version. Each paper is an individual piece of work with separate sections including: abstract, introduction, materials and experimental details, results and discussion, conclusions, and references. A failure analysis study was carried out on some specific mechanical components of diesel engines for industrial application. In order to increase the wear resistance of rocker arms, pushrods and valves, the deposition of ceramic coatings thermally sprayed was considered. Wear tests were performed on a plasma-sprayed ceramic coating in sliding motion against steel in order to understand the effect of a normal load applied, as well as the environmental conditions on the metal/ceramic coupling. Moreover, the influence of relative humidity on the tribological behaviour of two types of plasma-sprayed ceramic coatings and two types of HVOF-sprayed cermets in sliding motion against alumina, was evaluated through pin-on-disk testing. Different techniques for the microstructural examination were employed in this research study: Optical Microscopes (OM) and Scanning Electron Microscopes (SEM) with Energy Dispersive X-ray Spectroscopy (EDS) microprobe were used and also X-ray Diffraction (XRD) was carried out to describe the morphology of worn surfaces and to identify the main wear mechanisms involved. In addition, surface roughness, Vickers microhardness and fracture toughness measurements were performed in order to characterise the materials subjected to wear testing.

SOMMARIO

La corrosione, l'usura o l'effetto combinato di entrambi i meccanismi di danneggiamento rappresenta un costo per l'economia industriale di centinaia di miliardi di euro l'anno. Uno degli strumenti più efficaci per ridurre i danni dovuti a tali fenomeni è quello di trattare la superficie in maniera tale che essa possa svolgere delle funzioni differenti da quelle normalmente svolte dal solo materiale massivo. Per esempio, l'acciaio è un materiale assai utilizzato poiché poco costoso, resistente e semplice da produrre; tuttavia, esso è un materiale estremamente suscettibile alla corrosione in molti ambienti e pertanto necessita di essere rivestito allo scopo di garantire l'integrità dei componenti in acciaio durante il funzionamento. Elementi di piccole dimensioni possono essere verniciati, calorizzati, placcati o rivestiti con un materiale più resistente alla corrosione, mentre per parti che necessitano di elevata resistenza a corrosione e ad usura possono essere utilizzati rivestimenti spessi ottenuti mediante spruzzatura termica o film sottili. Infine, la difficoltà di manipolare elementi strutturali di grandi dimensioni ne limita i trattamenti eseguibili al fine di migliorarne le proprietà. Lo scopo dell'attività di ricerca presentata in questa tesi di dottorato è stato lo studio delle interazioni fra superfici di accoppiamento di tipo metallo/ceramico e di tipo metallo/metallo, per migliorare la resistenza ad usura di tali materiali soggetti a strisciamento reciproco. Il lavoro di tesi è presentato come collezione di tre articoli, alcuni già pubblicati e altri in fase avanzata di stesura. Ogni articolo include riassunto, introduzione, materiali e procedura sperimentale, risultati, conclusioni e riferimenti bibliografici.

L'attività principale ha riguardato uno studio dettagliato di *failure analysis* condotto su specifici componenti di motori diesel per applicazioni industriali. È stata in seguito considerata la possibilità di rivestire le superfici di bilancieri, aste e valvole mediante spruzzatura termica con l'intento di incrementarne la resistenza ad usura. Al fine di verificare la possibile efficacia dell'accoppiamento, un rivestimento ceramico con controparte in acciaio è stato sottoposto a prove di usura in condizioni variabili di carico applicato e umidità ambientale valutando l'influenza di tali parametri sul comportamento ad usura.

E' stata inoltre valutata, mediante prove di usura in configurazione pin-on-disk, l'influenza dell'umidità relativa sul comportamento tribologico di due rivestimenti al plasma e due rivestimenti spruzzati con tecnica HVOF con controparte in allumina.

Le analisi microstrutturali sono state eseguite attraverso l'uso di varie tecniche quali microscopia ottica (OM) ed elettronica a scansione (SEM) con microsonda EDS. La

diffrazione di raggi X (XRD) ha consentito di descrivere la morfologia delle superfici usurate e di identificare i principali meccanismi di usura coinvolti. I materiali soggetti a prove di usura sono stati inoltre caratterizzati attraverso prove di rugosità superficiale, microdurezza Vickers e tenacità a frattura.

TABLE OF CONTENTS

INTRODUCTION

The research activity that I carried out during my PhD and the main objectives of this thesis were to contribute to the knowledge of the tribological behaviour of metal/ceramic and metal/metal couplings.

The first part of my work was carried out in order to identify the causes of the wear damage observed at the rocker arm-pushrod and rocker arm-valve interfaces of diesel engines. Diesel engines are commonly used as mechanical engines and power generators in automobiles, locomotives, construction equipment, and many other industrial applications. In the second half of the 20^{th} century, the development of more fuel efficient and compact automobile engines with reduced environmental impact caused an increase in specific loads, speeds and temperatures of some engine components, such as the piston assembly, valve train and journal bearings. Moreover, the use of lower viscosity engine oils led to a decrease in thickness of the lubricant film between the interacting surfaces, reducing the operating time of the major frictional components. In the examined diesel engines, the replacement of mechanical tappets with hydraulic tappets increased the friction and wear between the coupling surfaces, reducing the operating time and need for additional maintenance. In some cases, the wear damage caused the seizure of the mechanical components.

Taking into account the main results obtained from the failure analysis performed on the diesel engines, I dealt with the improvement of the wear resistance of metal/ceramic couplings in the second part of my research activity. In particular, the deposition of ceramic coatings thermally sprayed on steels, was considered. The tribological behaviour of plasma-sprayed Cr_2O_3 coating against steel under different sliding wear conditions was evaluated through pin-on-disk testing. Compared to the loads that occur in diesel engine applications, relatively low normal loads were used because of the limitations of the test equipment. However, this can provide useful indications of the potential of the coating for use in sliding wear services. The effect of the environmental conditions on the wear mechanisms was also investigated.

Moreover, during my PhD I also studied the influence of relative humidity on the tribological behaviour of two types of plasma-sprayed ceramic coatings (Al_2O_3-$13TiO_2$ and Cr_2O_3) and of two types of HVOF-sprayed cermets (WC-12Co and Cr_3C_2-37WC-18Me). The coatings were subjected to pin-on-disk tests in sliding motion against alumina. The other parameters, such as normal load, sliding speed, test duration and temperature were assumed constant.

Most of the research activity is presented here as a collection of three articles. The manuscripts are:

Article 1

M. MERLIN, C. SOFFRITTI, R. VAZQUEZ, G. L. GARAGNANI, ***"Tribological characterisation of a diesel engine hydraulic tappets"*** Proceedings of 33° Convegno Nazionale AIM, Brescia, 10-12 November 2010.

Article 2

M. MERLIN, C. SOFFRITTI, R. VAZQUEZ, ***"Effect of relative humidity and applied loads on the tribological behaviour of a steel/Cr_2O_3-ceramic coupling"***, preprint, 2011.

Article 3

M. MERLIN, C. SOFFRITTI, R. VAZQUEZ, G. L. GARAGNANI, ***"Friction and wear behaviour of APS and HVOF advanced ceramic coatings"***, Proceedings of 33° Convegno Nazionale AIM, Brescia, 10-12 November 2010.

The following conclusions can be obtained from this PhD thesis:

- For the diesel engine studied in this work, the specific geometry of the rocker arm and pushrod causes an imbalance in the stresses acting on the rocker arm - valve and rocker arm - pushrod couplings. Moreover, the morphology of worn surfaces suggests the interaction of different wear mechanisms, such as abrasive and oxidational wear and surface fatigue. In particular, the abrasive wear is due to the presence of hard particles and soot contaminants observed on the contact surfaces. The effective depths and hardness values obtained at the rocker arm - pushrod and rocker arm - valve interfaces are different from the design specifications, because of the incomplete austenitization during hardening treatment and the partial removal of worn surfaces. The lack of homogenization during heat treatment is also confirmed by microstructural investigation.

- The influence of relative humidity on the tribological behaviour of metal-ceramic sliding pairs is strongly influenced by the normal load applied. In particular, for all the normal loads applied in dry conditions, metal/ceramic sliding-contact is associated with metallic film transfer (Fe_2O_3) onto the ceramic surface. The observations of the worn surfaces of the pins indicate a mild-oxidational wear mechanism with the appearance of ploughing and plastic deformation. The subsequent transition to severe-oxidational wear is associated with the localized melting of the oxide layer and its spreading onto the ceramic surface. As with the ceramic coating, the observations of Cr_2O_3 worn surfaces show that it undergoes microfractures along the splat and columnar grain boundaries. In wet conditions, the normal load applied influences the tribological behaviour. For higher normal loads the wear mechanisms are the same as those involved in dry conditions; for lower normal loads the moisture adsorbed can act as a protective layer preventing metal/ceramic interactions.

- The tribological behaviour of the investigated thermal-sprayed advanced ceramic coatings is influenced by relative humidity. In particular, the ceramic coatings (Al_2O_3-$13TiO_2$ and Cr_2O_3) are more sensitive to moisture than the cermet coatings (WC-12Co and Cr_3C_2-37WC-18Me). The SEM observations of the Al_2O_3-$13TiO_2$ worn surface show a non-protective tribolayer and the generation of surface microcracks with the consequent removal of wear debris in the form of flakes. The Cr_2O_3 worn surface appears smoother without evidence of significant wear and the pores remain open in the flattened surface. Many cracks are also propagated in the same direction as the normal load applied. WC-12Co coating is less sensitive to moisture due to the formation of oxide layers acting as a solid lubricant. Finally, the morphology of Cr_3C_2-37WC-18Me does not clarify the influence of relative humidity on the tribological behaviour of this coating.

ARTICLES

Article 1

TRIBOLOGICAL CHARACTERISATION OF A DIESEL ENGINE HYDRAULIC TAPPETS

CARATTERIZZAZIONE TRIBOLOGICA DI ACCOPPIAMENTI BILANCIERE-VALVOLA E BILANCIERE-ASTA DI MOTORI DIESEL PER MACCHINE INDUSTRIALI

Mattia Merlin, Chiara Soffritti, Reyna Vazquez, Gian Luca Garagnani

Department of Engineering - ENDIF
University of Ferrara
I-44122 Ferrara
Italy

Proceedings of 33° Convegno Nazionale AIM, Brescia, Italy, November 10-12, 2010

ABSTRACT

In this work is reported a research carried out to identify the causes of the wear damage at the rocker arm - pushrod and rocker arm - valve interfaces of diesel engines for industrial applications. In order to verify any design specification a Vickers microhardness tester and an optical microscope (OM) are used. The acquired micrographs are also elaborated by means of Image-Pro Plus v6.0 software for image analysis. The Scanning Electron Microscope (SEM) observations show the interaction of different wear mechanisms, such as abrasive wear, oxidational wear and surface fatigue. Finally, iron-based and titanium-based contaminants and soot particles are identified by means of Electron Dispersive Spectroscopy (EDS) microprobe.

KEYWORDS: Diesel engine; Induction hardening; Abrasive wear; Oxidational wear; Surface fatigue

1. INTRODUCTION

Diesel engines for industrial applications experience severe operating conditions, therefore the friction and wear can significantly reduce the operating time of the major frictional components. In particular, in the second half of the 20th century, many studies focused on the development of more fuel efficient and compact automobile engines with reduced environmental impact. This means, from the tribological point of view, an increase of specific loads, speeds and temperatures of some engine components, such as the piston assembly, the valve train and the journal bearings. Moreover, the use of lower viscosity engine oils led to a decrease of the lubricant film thickness between the interacting surfaces of these components [1].

Mackaldener and Lewis et al., highlighted that the cost of a diesel engine strongly depends on the consumer demands of long life and long service intervals; legislation and customers are also demanding lower emissions. Meeting these requirements promoted the development of many new technologies for removal of the soot particles. For example, the use of performance-enhancing additives can disperse the increasing soot and reduce the friction between the engine components. However, the soot is maintained in suspension by the dispersant additives of the lubricant. As soot levels increase, the viscosity of the oil also increases. At high levels, this suspended soot can become abrasive and can result in wear of the contact surfaces [4-10]. The optimisation of the tribological systems is therefore important for the design of all engine components in relative sliding motion. Simulation is a very useful tool for predicting the friction and wear behaviour of the mechanical systems, like the cam mechanism. Spiegelberg and Andersson used a rigid body mechanics model to analyse the relative motion in the coupling surfaces between rocker arm pad and valve bridge. The surface velocities obtained were then used for the simulation of friction and wear of the sliding surfaces, using a Coulomb friction model. The results showed that both the maximum wear depth and wear distributions are significantly influenced by the wear pad radius and the position of the wear pad radius centre relative to the rocker arm bearing centre [11].

Failure analysis is another very important tool for understanding the mechanism and causes of the failure of engineering parts or components. It can be defined as the examination of a failed component and of the failure situation in order to determine the causes of the inability of a component to perform properly its function. It can provide information for improvements in operating procedures and design of new or existing devices, systems or structures. Z.W. Yu and X.L. Xu showed a failure analysis of two diesel engine rocker arms made of a C45 steel.

They found the failure in service was due to the spheroidisation of cementite in pearlite in the entire matrix and in a banded microstructure in the crack initiation region [12]. Ching-Sung Chung and Ho-Kyung Kim used the results of the failure analysis, conducted on a rocker arm made of cast aluminum ALDC8, for a Finite Element Modelling (FEM) analysis in order to evaluate the fatigue performance [13].

The research activity presented in this work is carried out to identify the causes of the wear damage at the rocker arm - pushrod and rocker arm - valve interfaces of diesel engines for industrial applications. In the examined diesel engines the replacement of mechanical tappets with hydraulic tappets increases the friction and wear between the coupling surfaces, reducing the operating time and requiring supplementary maintenance. In some cases, the wear damage caused the seizure of the mechanical components. The morphology of worn surfaces is investigated by preliminary macroscopic observations, while the microstructural investigation is carried out by means of an Optical Microscope (OM). A Scanning Electron Microscope (SEM) with Electron Dispersive Spectroscopy (EDS) microprobe is also used in order to identify the wear mechanisms and the presence of contaminants and soot particles. Any design specification is verified by Vickers microhardness measurements.

2. MATERIALS AND EXPERIMENTAL DETAILS

All the investigated mechanical components are made in steel. The chemical compositions are evaluated by means of Optical Emission Spectroscopy (OES) and the main results are collected in Table I.

Table I – Chemical compositions (wt.%) of the steels.

Components	C	S	Mn	Si	Cr	Ni	Mo	Cu	Fe
Rocker arm	0.42	0.020	0.71	0.16	0.13	0.08	<0.03	0.17	bal.
Pushrod	0.37	<0.002	0.67	0.20	0.19	0.07	0.06	0.14	bal.
Intake valve	0.88	<0.002	0.60	0.61	16.15	0.13	1.75	0.05	bal.
Exhaust valve	0.50	0.006	0.47	3.34	7.68	0.13	0.03	0.03	bal.

Rocker arm, pushrod and valves are subjected to an induction hardening treatment in order to increase the surface hardness and wear resistance. The design specifications related to effective depths and hardness values required at the rocker arm - pushrod and rocker arm - valve interfaces are listed in Table II.

Table II – Design specifications of the induction hardening treatment.

Component	Effective depth [mm]	Hardness [HRC]
Rocker arm	2	55-59
Pushrod*	---	≥ 58
Intake valve	0.8	≥ 48
Exhaust valve	0.8	≥ 54

* An effective depth is not defined because the head of the pushrod is entirely hardened.

The mechanical components analysed are part of a four-cylinders diesel engine. In total, four couples of rocker arms, pushrods, intake valves and exhaust valves are studied. In particular, the investigated surfaces are the portions of rocker arms in contact with valves/pushrods and the regions of valves/pushrods in contact with rocker arms. Macroscopic analyses are carried out by means of a LEICA MZ6 microscope in order to observe, at low magnifications, the morphology of the worn surfaces. The materials are also characterised by Vickers microhardness measurements, performed with a Microhardness Tester FM Future-Tech and with a load of 1 kg_f. Each component is sectioned in longitudinal and transversal direction, the samples obtained are subjected to metallographic analysis by an optical microscope LEICA MEF4M equipped with image analysis software Archive4Images v.3.20b. The ImagePro Plus v6.0 software for image analysis is used to determine the content of the phases formed as a result of the induction hardening treatment. In order to identify the wear mechanisms rocker arms, pushrods and valves are studied by a ZEISS EVO 40 Scanning Electron Microscope (SEM) with Energy Dispersive Spectroscopy (EDS) microprobe.

3. RESULTS AND DISCUSSION

3.1 Macroscopic observations

In Figure 1 are reported two macrographs of surface conditions at the rocker arm - exhaust valve interface. Generally, wear is more severe at the discharge due to the high exhaust temperatures and contact pressures. As can be seen, the rocker arm and exhaust valve worn surfaces can be divided in two regions: the first one, having a bright appearance, is characterised by reddish scoring probably caused by abrasive and oxidational wear mechanisms. In the second one, less extensive and with an opaque appearance, many pits compatible with a surface fatigue mechanism are observed. Moreover, on the rocker arm worn

surface the wear is deeper at the region more distant from the rocker arm shaft support (arrow in Figure 1a). This behaviour is due to the pushrod inclination and to the misalignment between the portion of rocker arm in contact with valve and the region of rocker arm in contact with pushrod. The particular geometry of these components results in an imbalance of the stresses acting on rocker arm - exhaust valve coupling and therefore in an irregular wear damage. Finally, in Figure 1b is can be noted that the exhaust valve has not rotated, which corresponds to a malfunction of the component in service.

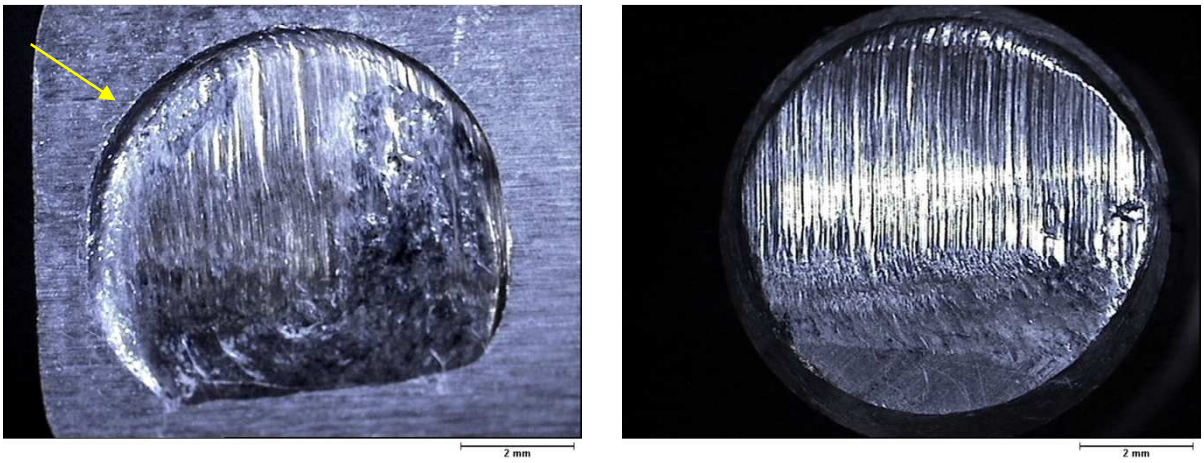

(a) (b)

Figure 1 - Wear damage at the rocker arm - exhaust valve interface: (a) rocker arm, (b) exhaust valve.

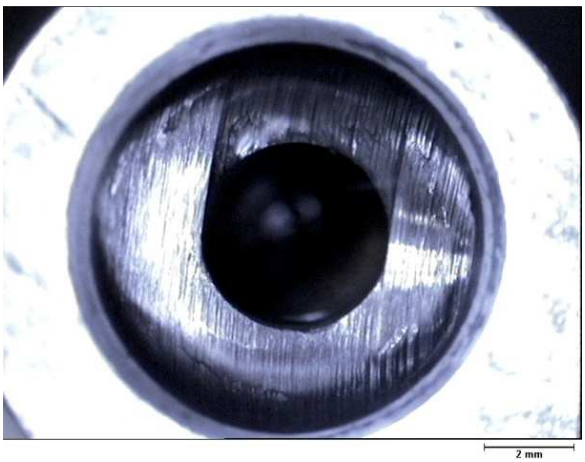

Figure 2 - Wear damage of the rocker arm at the rocker arm - pushrod interface.

In Figure 2 is depicted the wear damage on the rocker arm at rocker arm - pushrod interface. The wear mechanisms are the same highlighted in Figure 1a and 1b. The wear is non-uniformly distributed and on the worn surfaces scoring and pits are visible.

3.2 Microstructural analysis

In this section are summarised the main results of the microstructural investigation performed by the optical microscope (OM). The components are sectioned in longitudinal and transversal directions: the samples obtained are polished and subsequently etched by the Nital4 chemical solution, in agreement with ASTM E407-99 standard.

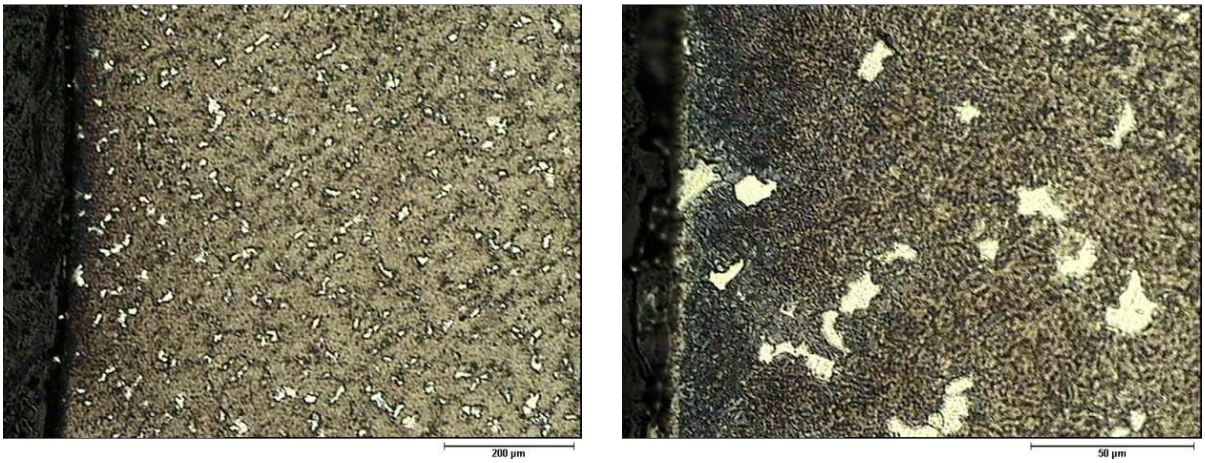

(a) (b)

Figure 3 - Optical micrographs of rocker arm hardened zone at the rocker arm - exhaust valve interface: (a) 100x, (b) 500x.

Microstructural analyses carried out on the induction - hardened surfaces of rocker arms and pushrods show a martensitic microstructure with a great amount of ferrite. In particular, optical micrographs in Figure 3 depict the microstructure of rocker arm hardened zone at the rocker arm - exhaust valve interface. At the rocker arm - pushrod interface ferrite is also non-uniformly distributed; this behaviour is due to an incorrect induction hardening treatment and to an inadequate inductor geometry. The content of the phases, formed as a result of the induction hardening treatment, is determined by the ImagePro Plus v6.0 software for image analysis. The obtained values are discussed in section 3.2.1. Moreover, in the regions more distant from the hardened surfaces the microstructure of rocker arm is ferritic-pearlitic with lamellar-type pearlite, while the microstructure of pushrod is ferritic-pearlitic with spheroidal-type pearlite. The authors suggest that the spheroidization of cementite in pearlite promotes the complete austenitization during hardening treatment and prevents the formation of ferrite in heat-treated surfaces.

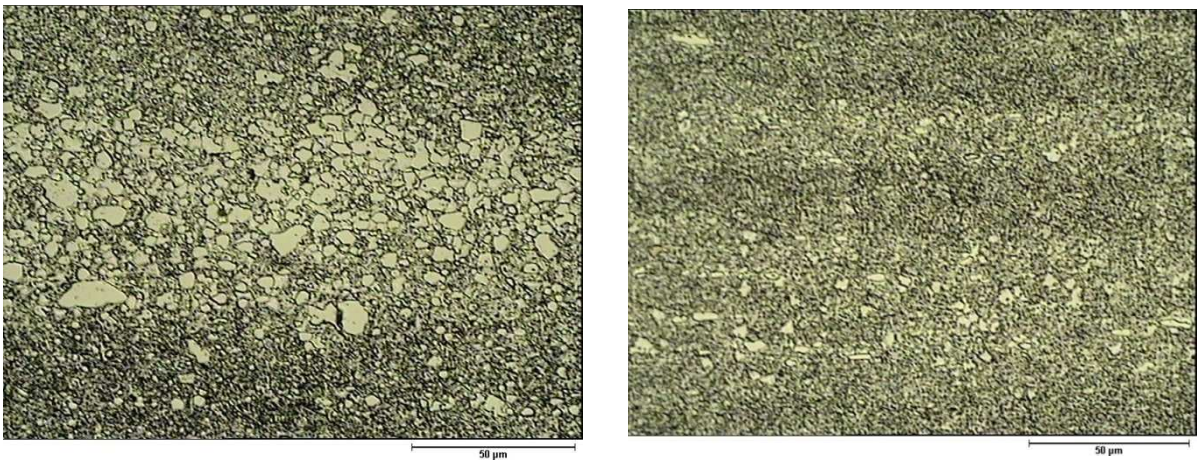

(a) (b)

Figure 4 - Optical micrographs of the valves: (a) intake valve, (b) exhaust valve.

As concern the valves, in Figure 4a and 4b are shown the optical micrographs of an intake valve and an exhaust valve, respectively. In both cases, the microstructural investigation highlights a great amount of coarse carbide particles, probably chromium-based carbides, oriented along one preferred direction. Many fine carbide particles are also visible at the grain boundary. The largest amount of carbides observed in Figure 4a is related to the highest content of chromium and molybdenum in the intake valve (see Table I in section 2). The presence of these particles in the regions near the coupling surfaces causes an increase in abrasive wear of the rocker arm.

3.2.1 Image analysis

In this section are discussed the main results of image analysis performed in order to determine the content of martensite and ferrite in the induction-hardened surfaces of rocker arm and pushrod. In particular, the regions investigated are: the portions of rocker arm in contact with valve/pushrod and the region of pushrod in contact with rocker arm. For each zone a mean of four optical micrographs, representative of the ferrite distribution, are selected. By ImagePro Plus v6.0 software for image analysis, the optical micrographs are processed and properly contrasted to discriminate martensite from ferrite and to calculate the percentage of both phases. For example, in Table III are collected the percentages of martensite and ferrite in the hardened surfaces of a rocker arm at the rocker arm - pushrod interface. As can be seen, in some cases the amount of ferrite is very high (about 10%); it is also non-uniformly distributed, as mentioned in section 3.2.

Table III - Content of martensite and ferrite in a rocker arm hardened surface.

Martensite [%]	Ferrite [%]
93	7
97	3
90	10
96	4

The image analysis carried out in the hardened surfaces of rocker arms at the rocker arm-valve interface and in the induction hardening region of pushrods shows a content of ferrite approximately constant and equal to about 4÷5%.

3.3 Microhardness measurements

Vickers microhardness tests (HV_1) are performed in order to verify the design specifications related to effective depths and hardness values required at the rocker arm - pushrod and rocker arm - valve interfaces, in accordance with UNI EN ISO 6507-1:2006 standard. The Vickers microhardness values are obtained as average of five valid measurements and converted to Rockwell hardness (HRC) by interpolation, in agreement with ASTM E140-07 standard.

Figure 5a and 5b depict the microhardness profiles of the rocker arm induction-hardened surfaces at the rocker arm - valve and at the rocker arm - pushrod interface, respectively. In both cases, the effective depth is lower than the 2 mm required by design specifications; it can be due to an incomplete austenitization during hardening treatment (see section 3.2) and to the partial removal of worn surfaces. The microhardness profile of the rocker arm induction-hardened surface at the rocker arm - pushrod interface (Figure 5b) shows some irregularities probably caused by a lack of homogenization during heat treatment. The microhardness is nearly constant up to a distance of about 3 mm from the hardened surface; therefore, at a distance of 2 mm from the hardened surface (see design specifications in Table II) the values obtained are higher than the microhardness typical of a ferritic-pearlitic microstructure. These results confirm the use of an inadequate inductor geometry during execution of the induction hardening treatment.

Also the microhardness measurements on the pushrod hardened surface are lower than the 58 HRC required by design specifications. However, the calculated values are approximately constant, in accordance with the negligible content of ferrite in the induction-hardened surfaces (see section 3.2).

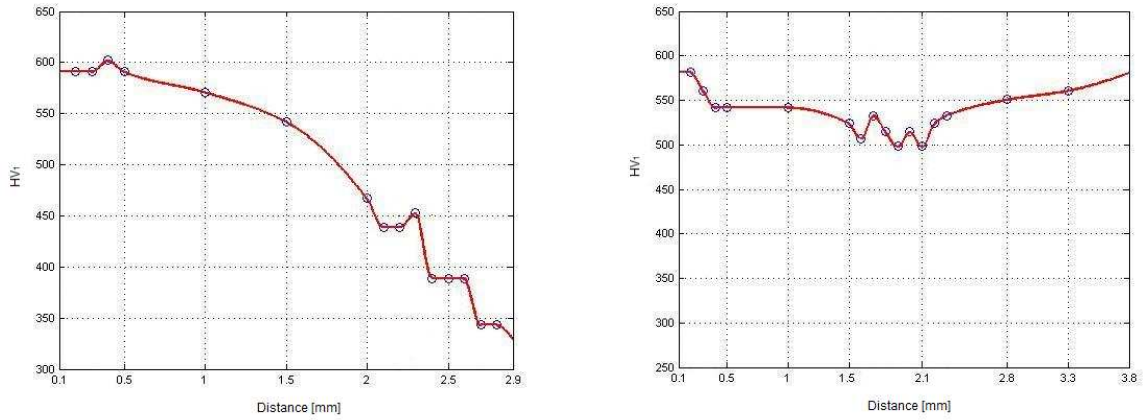

(a) (b)

Figure 5 - Microhardness profiles on a rocker arm: (a) rocker arm - valve interface, (b) rocker arm - pushrod interface.

3.4 SEM analysis of worn surfaces

In Figure 6 are reported the SEM micrographs of the wear damage observed on a pushrod. In particular, Figure 6a shows an overview of the worn surface. Deep grooves compatible with an abrasive wear mechanism are visible; this behaviour is principally due to the presence of wear debris and hard particles, as result of lubricating oil contamination, entrapped between the coupling surfaces. At higher magnification (Figure 6b), the local plastic deformation and the subsequent generation of wear debris in the form of flakes are also evident. Figure 7 depicts the detail of a wear debris and corresponding EDS analysis results. EDS analysis highlights that the particle contents a great amount of titanium; consequently, it can be considered a residual of machining performed on the mechanical components, which form the rocker arm - pushrod coupling.

An overview of the morphology of a rocker arm worn surface at the rocker arm - valve interface is observed in Figure 8a; many pits due to a surface fatigue mechanism can be clearly seen. The local plastic flow at the rocker arm - valve interface promotes the fatigue cracks initiation, while the lubricating oil seepage inside the cracks can significantly accelerate the fatigue cracks growth [14]. In Figure 8b is shown a detail of the beach marks corresponding to different stages of the load history. Moreover, the presence in surface or sub-surface layers of non-metallic inclusions and, generally, of irregularities in the matrix (e.g. ferrite, see section 3.2) greatly affects initiation and growth of fatigue cracks.

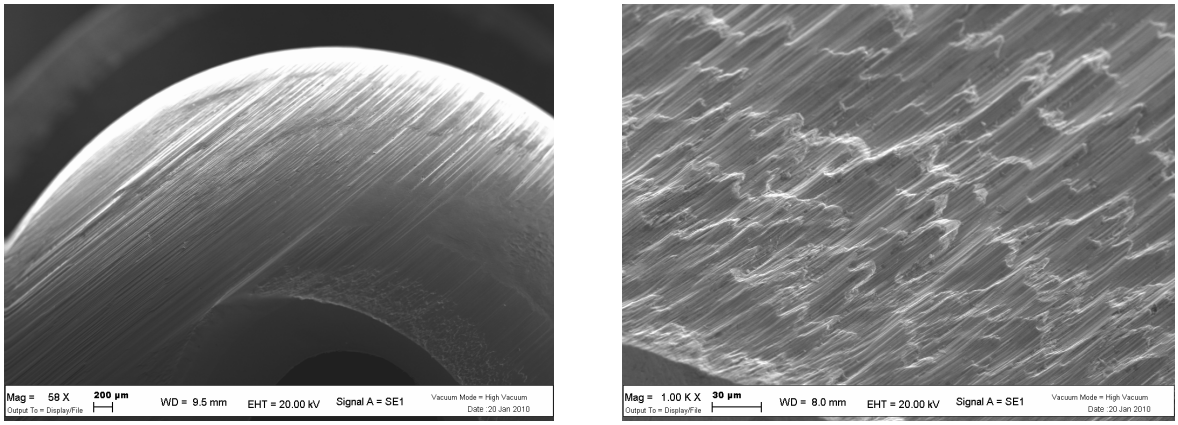

(a) (b)

Figure 6 - SEM micrographs of the wear damage observed on a pushrod: (a) overview of the worn surface, (b) detail at higher magnification.

Inside the pits highlighted in Figure 8 many rounded particles are also observed. EDS analysis shows they are mainly iron oxides, compatible with an oxidational wear mechanism. Figure 9 depicts one rounded particles and the corresponding EDS analysis results.

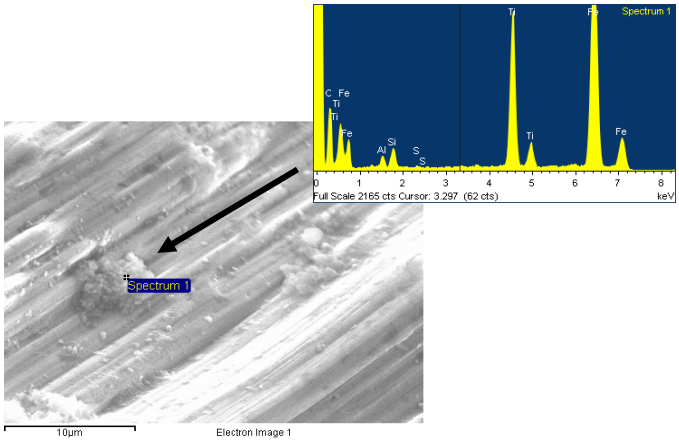

Figure 7 - SEM micrographs of a wear debris and corresponding EDS analysis.

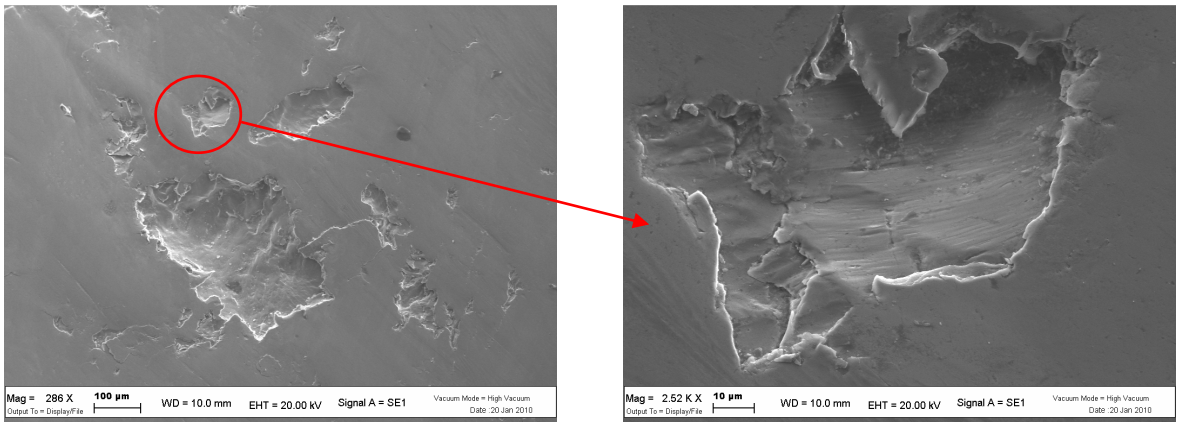

(a) (b)

Figure 8 - SEM micrographs of the wear damage observed on a rocker arm at the interface rocker arm - valve: (a) overview of the worn surface, (b) detail at higher magnification.

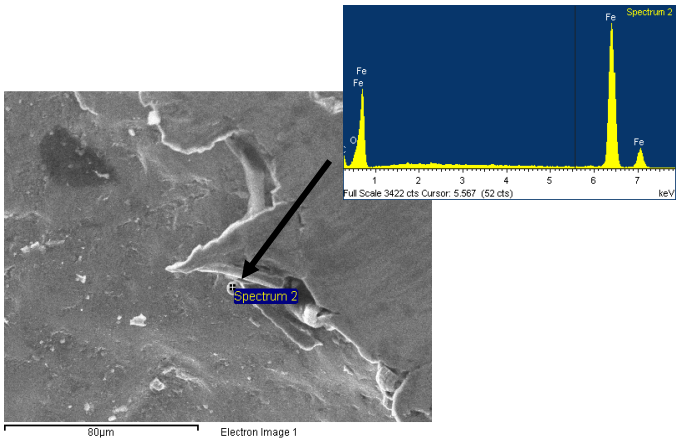

Figure 9 - SEM micrographs of a rounded particles and corresponding EDS analysis.

As concern the valves, on the worn surfaces represented in Figure 10 scoring due to the abrasion, produced by wear debris and hard particles, is visible. The presence of coarse carbides in the regions near the coupling surfaces, highlighted by microstructural analysis (see section 3.2), promotes an increase in abrasive wear of the rocker arm - valve coupling surfaces (Figure 10a). The details in Figure 10b and 10c report many pits caused by surface fatigue and soot contaminants spread on the exhaust valve surface, respectively. In particular, soot particles on the contact surfaces are identified by EDS analysis.

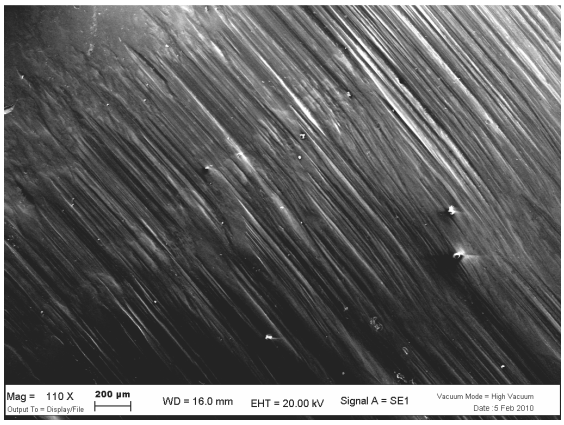

(a)

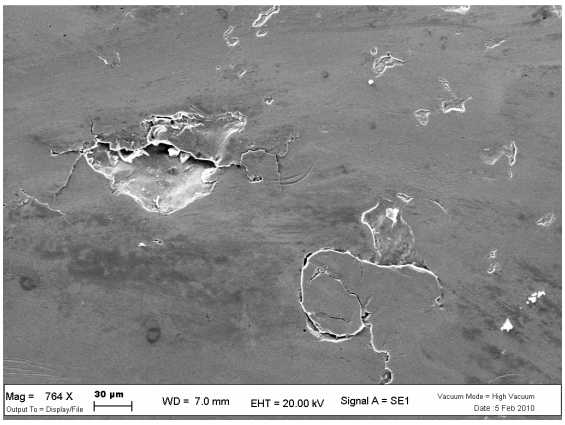

(b)

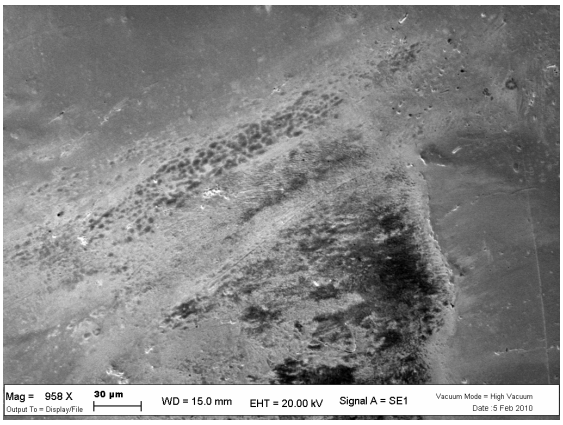

(c)

Figure 10 - SEM micrographs of the wear damage on the exhaust valve surface: (a) detail of scoring, (b) pits due to surface fatigue, (c) soot contaminants.

4. CONCLUSIONS

Based on main results of the analyses performed in order to identify the causes of the wear damage at the rocker arm - pushrod and rocker arm - valve interfaces, the following conclusions can be drawn:

- The pushrod inclination and the misalignment between the portion of rocker arm in contact with valve and the region of rocker arm in contact with pushrod, cause an imbalance of the stresses acting on rocker arm - exhaust valve coupling and therefore an irregular wear damage. In particular, on the rocker arm worn surface the wear is deeper at the region more distant from the rocker arm shaft support. The morphology of worn surfaces suggests the interaction of different wear mechanisms, such as abrasive wear, oxidational wear and surface fatigue.

- In the portions of rocker arm subjected to the induction hardening treatment and in the regions nearly the contact surfaces a great amount of ferrite is observed. It is probably due to the use of an inadequate inductor geometry and to the presence of a ferritic-pearlitic microstructure with lamellar-type pearlite.

- Microhardness profiles confirm the lack of homogenisation during heat treatment. In many cases, the effective depths and hardness values obtained at the rocker arm - pushrod and rocker arm - valve interfaces are different from design specifications, because of the incomplete austenitization during hardening treatment and the partial removal of worn surfaces.

- In the contact surfaces many wear debris and soot contaminants are observed. On the pushrod worn surface is also noted a titanium-rich particle, as result of machining performed on the mechanical components, which form the rocker arm - pushrod coupling. The authors suggest that these contaminants, in the form of hard particles, promote the abrasive wear of the contact surfaces.

REFERENCES

1) M. PRIEST, C.M. Taylor, Automotive engine tribology – approaching the surface, Wear 241, (2000), p. 193-203
2) M. MACKALDENER, Simulations in engine design with focus on tribology, Proceedings of the 10th Nordic Symposium on Tribology, Nordtrib 2002, TRITA-MMK 2002:03, (2002)
3) R. LEWIS et al., Design and development of a bench test rig for investigating diesel engine inlet valve and seat insert wear, Proceedings Austrib '98, Brisbane, Australia, (1998)
4) S. ANTUSCH et al., On the tribochemical action of engine soot, Wear 269, (2010), p. 1-12
5) S. GEORGE et al., Effect of diesel soot contaminated oil on engine wear, Wear 262, (2007), p. 1113-1122
6) M. GAUTAM et al., Effect of diesel soot contaminated oil on engine wear – investigation of novel oil formulations, Tribology International 32, (1999), p. 687-699
7) P. DIATTO et al., Investigation on soot dispersant properties and wear effects in the boundary lubrication regime, Tribology Series 36, (1999), p. 809-819
8) E.A. KHORSHID, A.M. NAWWAR, A review of the effect of sand dust and filtration on automobile engine wear, Wear 141-2, (1991), p. 349-371
9) J.A. LENG, J.E. Davies, Ferrographic examination of unused lubricants for diesel engine, Wear 122-1, (1988), p. 115-119
10) M. KAWAMURA et al., Deterioration of antiwear properties of diesel engine oils during use, Wear 122-3, (1988), p. 269-280
11) C. SPIEGELBERG, S. ANDERSSON, Simulation of friction and wear in the contact between the valve bridge and rocker arm pad in a cam mechanism, Wear 261, (2005), p. 58-67
12) Z.W. YU, X.L. Xu, Failure analysis of diesel engine rocker arms, Engineering Failure Analysis 13, (2006), p. 598-605
13) C.S. CHUNG, H.K. KIM, Safety evaluation of the rocker arm of a diesel engine, Material & Design 31, (2010), p. 940-945
14) G. STRAFFELINI, Attrito e usura: metodologie di progettazione e controllo, Tecniche nuove, (2005)

Article 2

EFFECT OF RELATIVE HUMIDITY AND APPLIED LOADS ON THE TRIBOLOGICAL BEHAVIOUR OF A STEEL/Cr_2O_3-CERAMIC COUPLING

Mattia Merlin, Chiara Soffritti, Reyna Vazquez

Department of Engineering - ENDIF
University of Ferrara
I-44122 Ferrara
Italy

Preprint 2011

ABSTRACT

The friction and wear behaviour of a carbon steel in sliding contact with a plasma-sprayed ceramic coating (Cr_2O_3) is investigated under different conditions of normal load and relative humidity, through a pin-on-disk equipment. The samples are analysed by means of Optical Emission Spectroscopy (OES), Optical Microscope (OM), Scanning Electron Microscope (SEM) with Energy Dispersive Spectroscopy (EDS), X-ray Diffraction (XRD), surface roughness, fracture toughness and microhardness tester. During tests, friction was continuously monitored while the wear rate of coatings was evaluated by measurements of wear scar profiles after the tests. The wear rate of the pins was determined by weighting them before and after the wear tests. For all the normal loads applied in dry conditions, the metallic film transfer onto ceramic surface was observed. In wet conditions, metal transfer was greatly depending on the normal load applied. On Cr_2O_3 wear scars microcracks along splat and columnar grains boundaries were distinguished. The observations of the worn surfaces of the pins indicate a mild-oxidational wear mechanism with the appearance of ploughing and plastic deformation

KEYWORDS: Diesel engine; Steel; Plasma-spray coating; Friction; Wear; Metal transfer.

1. INTRODUCTION

In the last decade many efforts are made to improve the performance of diesel engine in terms of fuel efficiency and low emissions. These include the possibility to operate on engine subsystems like the engine block with its pistons and cylinders, the transmission, fuel system, the valve train and the exhaust system. Many studies concern the use of multi-component alloys in valves and valve seats [1-3]. Such alloys are resistant to high temperatures and in corrosive environment of combustion gases but are very expensive. For example, Stott et al. investigated the effect of high-temperature oxidation on the sliding wear of superalloys [4-6]. They dealt with the ability of so-called 'glaze' layers to protect the surfaces during sliding wear at high temperatures and under relatively low loads and sliding speeds.

It is well-known that heat, either frictional or externally applied, has a great influence on the wear processes of metallic components. High temperatures can facilitate oxidation of the contacting surface, causing considerable decrease in wear rate and giving a transition from severe to mild wear. This change is usually associated with the generation of oxide and partially-oxidized metal debris on the mating surfaces. At higher temperatures a glaze, a top layer of compacted particles, can form on the surface reducing friction and wear rates. However, when the sliding speed at room temperature is very high, the removal of the oxide glaze can occur, leading to severe-oxidational wear [7-10]. The capability of this oxide to give protection against the wear damage by acting as a barrier is due to the rate of diffusion of the reactants across the barrier layer. On exposure to air at temperatures upward of 500°C iron and mild steel form protective glazes (tribo-layers) of Fe_3O_4. These are effective barriers to diffusion, but the phase FeO becomes stable at higher temperatures. It develops at the metal/ Fe_3O_4 scale interface and is a poor barrier to diffusion of reactants [11, 12].

The effects of oxygen in reducing wear of metallic components have been investigated for many years. However, in practical applications also the humidity greatly affects the wear rates of metals. Some authors proposed that increasing humidity inhibits the delamination and adhesion wear of steels. They suggested it is due to the reduction of the oxidation rate on the steel worn surface and to the formation of iron hydroxide and ferri-oxide-hydrate. These oxides and the water adsorption act as protective layers preventing metal/metal interaction [13, 14]. Goto and Buckley found the opposite, which is a direct correlation between wear and humidity: the lack of oxygen adsorption in the presence of water vapour can reduce the rate of oxidation and thus increase the wear [15]. On the other hand, Bregliozzi et al. found both the

wear and friction coefficient for un-lubricated sliding of stainless steel significantly dropped, though the oxidation rate reduces with increasing humidity [15, 16]. Finally, other authors demonstrated that the sliding speed significantly influences the effect of humidity in sliding wear of steels: at high sliding speed, the wear increases with humidity, while a converse of this situation is observed at low sliding speed [17].

An interesting alternative to the use of ferrous alloys or superalloys in engine subsystems is the employment of ceramic coatings thermally sprayed on cheaper and shock resistant materials, such as carbon steels. Some ceramics have already found engineering applications as tribological components like cutting tool inserts, rolling bearings, braking devices, water pumps, ash scrapers, cylinder head fire decks, piston crowns, exhaust valve faces and so on [18]. Moreover, thermal-sprayed coatings are resistant to many corrosive environments, they possess chemical stability and very high hardness and they can stand high temperatures. However, the choice of suitable coatings is difficult. In literature many studies investigated the friction of hard materials, such as ceramics against steels [19-23]. They examined the existence of many cracks at the metal surface or the formation of grooves and wear debris with subsequent metal removal. The metal particles were transferred onto the ceramic by adhesion. Only scratches due to plastic deformation were seen on the ceramic surface. It was also shown that the transfer between metal and ceramic depended on the load (more precisely on the Hertzian pressure) and on the temperature at the interface. It also depended on the specific properties of the ceramic, like its hardness, its roughness, its affinity with the metal, the cohesion among grains and the tensile strength of the antagonist. Fernandez et al. evaluated the wear behaviour of plasma-sprayed Cr_2O_3 coatings against steel in a wide range of loads and sliding speeds. The results demonstrated the wear of the coatings increased with increasing load. Moreover, in dry sliding of the Cr_2O_3 coating there existed a minimum-wear sliding speed (about 0.5 m/s) and a maximum-wear sliding speed (about 3 m/s) [24].

The aim of this work is to evaluate the tribological behaviour of the plasma-sprayed Cr_2O_3 coating against a carbon steel under different sliding wear conditions, through pin-on-disk testing. Compared to the loads that occur in diesel engine applications, relatively low normal loads are used because of the limitations of the test equipment. However, this can provide useful indications of the potential of the coating for use in sliding wear services. All tests are carried out at room temperature and at 15% and 95% of relative humidity. The effect of both the environmental conditions and the applied load on the wear mechanisms is discussed.

2. MATERIALS AND EXPERIMENTAL DETAILS

A plasma-sprayed Cr_2O_3 ceramic coating with a thickness of 150 μm (powder: Amperit®, -45 +22.5 μm, fused and crushed) on an about 20 μm-thick Ni-20%Cr bond coat (powder: Metco 43CNS, -106 +45 μm) to improve the ceramic material adhesion, are deposited onto circular steel plates (80 mm in diameter and 6 mm in thickness). The spray parameters are confidential. The chemical composition of the steel plates was determined by Optical Emission Spectroscopy (OES), whereas the composition of the feedstock powder was directly provided by the manufacturer. Details of the steel plates and feedstock powders chemical composition are reported in Table 1.

Table 1 - Steels and feedstock powders used to produce top and bond coatings.

	Composition
Cr_2O_3	0.06% SiO_2; 0.03% Fe_2O_3; <0.02% TiO_2; balance Cr_2O_3
Ni-20%Cr	19.07% Cr; 1.1% Si; 0.4% Fe; 0.02% C; balance Ni
Disk	0.22% C; 0.88% Mn; 0.87% Ni; 0.84% Cr; 0.30% Si; 0.20% Cu; 0.06% Mo; 0.03% S; 0.02% V; 0.02% P; balance Fe
Pin	0.23% C; 0.86% Mn; 0.95% Ni; 0.91% Cr; 0.26% Si; 0.10% Cu; 0.06% Mo; 0.02% S; 0.02% V; 0.01% P; balance Fe

The coating microstructure was investigated by a Philips X'PERT PW3050 diffractometer, using Cu Kα radiation (λ=1.54 Å), with an intensity scanner vs. diffraction angle between 15° and 120° (step size of 0.06°, scanner velocity of 2 s/step and 1.5 grid), a voltage of 40 kV and a 30 mA filament current. The LEICA MEF4M Optical Microscope on properly polished cross-sections was also employed. The micrographs were elaborated by means of Image-Pro Plus v6.0 image analysis software to evaluate coating porosity. Roughness parameters (R_a and R_z) were calculated by the portable Handysurf E35_A ZEISS-TSK rugosimeter. Before each measurement all the coating surfaces were cleaned by ultrasonic bath. Microhardness (3 N load and 15 s loading time) and fracture toughness (10 N load) measurements were performed on polished cross-sections of the coating by means of a Future-Tech FM-model Vickers microindenter. A mean of 15 indentations were carried out for each microhardness and toughness measurement. In particular, fracture toughness was evaluated by measures of the indentation diagonals and crack lenghts from optical micrographs, employing the Evans-Wilshaw equation:

$$K_{IC} = 0.079(P/a^{3/2})log(4.5a/c) \quad (1)$$

where a is the half diagonal of the indentation (μm), c is the crack length (μm) and P is the load (mN). This formula is developed for "half-penny-shaped" cracks, but in literature is reported it is valid also for Palmqvist cracks. Unique limitation is that the ratio between the crack and the half diagonal length must be between 0.6 and 4.5 [25, 26].

Pin-on-disk dry sliding tests were performed with a Multispecimen Tester tribometer produced by DUCOM Instruments, in accordance with ASTM G99-05 "Standard test method for wear testing with a pin-on-disk apparatus", using cylindrical steel pins of 6 mm in diameter and 22 mm in height as counterpart material. The chemical composition of the pin is listed in Table 1. All the surfaces of the pin were cemented for about 500 μm in thickness. The Vickers microhardness of the pins was determined (1 N load and 15 s loading time) on cleaned cross-sections, at a distance of 100 μm from the coupling surface. Four different sets of tribological parameters were employed, varying the normal load and relative humidity (RU). In particular, normal loads were fixed at 450 N and 650 N respectively, whereas the values of 15% and 95% of the relative humidity were selected. For each test, the sliding speed of 1 m/s and the sliding distance of 7500 m were maintained constant. All tests were carried out at room temperature. Equipment directly calculated the friction coefficient. The wear rate of pins were evaluated by weighting the specimens before and after the tests. Weight loss was converted to volume loss by dividing it by the density of the material. Wear rate of disks were evaluated by measuring the area of the wear track cross-section by a Hommelwerk T2000 profilometer. Each area, obtained as an average value of four measurements along the wear circumference, was used to calculate the wear volume. In order to understand the main wear mechanisms, the coating worn surfaces were investigated by means of X-ray Diffraction (XRD), Scanning Electron Microscope (SEM) and Energy Dispersive Spectroscopy (EDS) microprobe. The pin worn cross-sections were characterised by OM and SEM analyses and Vickers microhardness measurements.

3. RESULTS AND DISCUSSION

3.1 Microstructure and mechanical properties

In Figures 1a and 1b are reported two optical micrographs of the investigated Cr_2O_3 coating showing the typical lamellar microstructures of a plasma-sprayed ceramic coating. It is characterised by a homogeneous microstructure with a prevalence of inter-lamellar cracks and uniformly distributed pores. Inter-lamellar cracks, caused by thermal residual stresses, are the main reason for the low intersplat cohesion exhibited by the coating. The Ni-20%Cr bond coat is markedly irregular in order to facilitate the adhesion of the coating to the substrate (Figure 1a). At higher magnification the optical micrograph of the steel/bond coat interface shows the evidence of pores and sandblast residues (Figure 1b). The coating porosity determined by image analysis is about 9%, due to splat stacking faults and gas entrapment [27]. The XRD analysis of the coating cross-section, depicted in Figure 2, reveals it is fully consisted in eskolaite phase (Cr_2O_3). Hardness, roughness parameters and fracture toughness of the coating are listed in Table 2. After the Vickers indentations for the measurement of fracture toughness, micrographs of the coating cross-sections showed that crack preferentially propagate along splat boundaries, parallel to the substrate interface. It is a further evidence of the low intersplat cohesion.

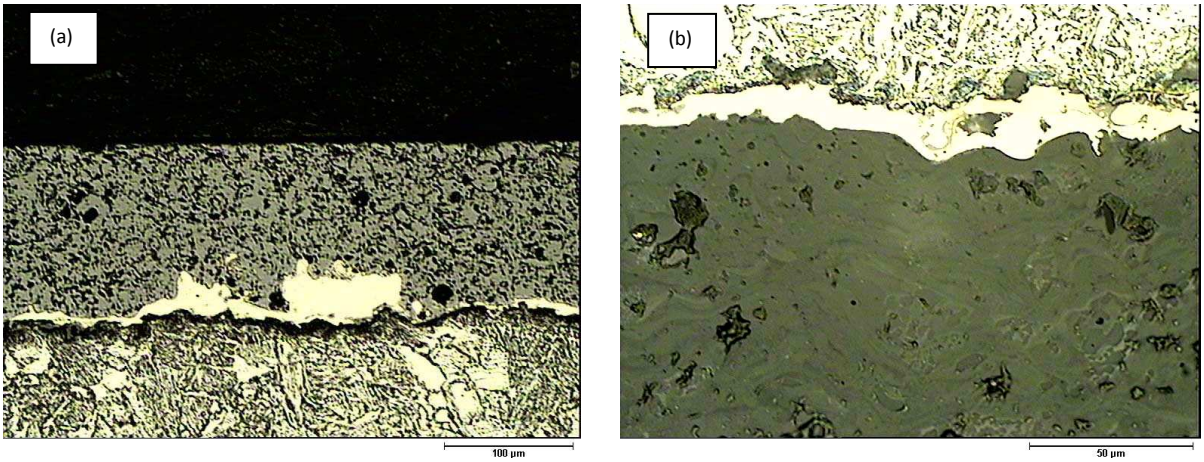

Figure 1 - Optical micrographs showing cross-sections of Cr_2O_3 coating and Ni-20%Cr bond coat.

Micrographs collected in Figures 3a and 3b describe the microstructure of a steel pin near the coupling surface. Figure 3a allows to evaluate a thickness of the hardened layer of about 500 μm. At higher magnification the cemented layer exhibits a martensitic microstructure with a

little amount of carbides (Figure 3b), whereas the unaffected material possesses a homogeneous lower bainitic microstructure. Vickers microhardness of the martensitic + carbide microstructure, near the coupling surface, is listed in Table 2.

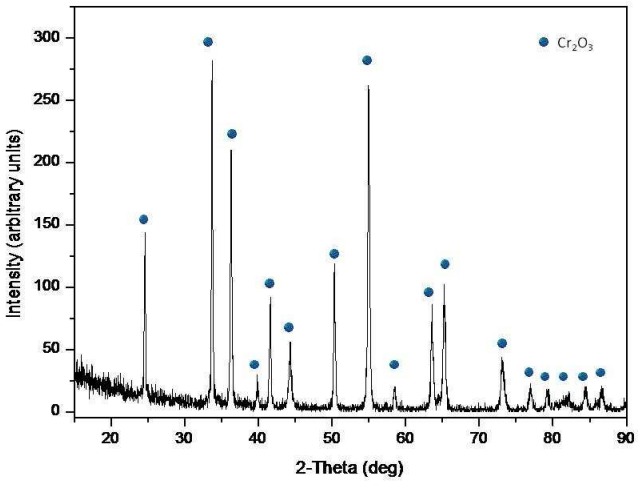

Figure 2 - XRD pattern of Cr_2O_3 coating.

Table 2 – Mechanical properties and roughness of the ceramic coating and of the steel pins.

	HV_{1N} [GPa]	HV_{3N} [GPa]	R_a [μm]	R_z [μm]	K_{IC} [MPa·$m^{1/2}$]
Cr_2O_3	-----	11.88 ± 0.45	0.15 ± 0.02	1.78 ± 0.19	3.07 ± 0.71
Pins	6.70 ± 0.05	-----	-----	-----	-----

* Vickers microhardness is evaluated on the pin cross-section, at a distance of 100 μm from the coupling surface.

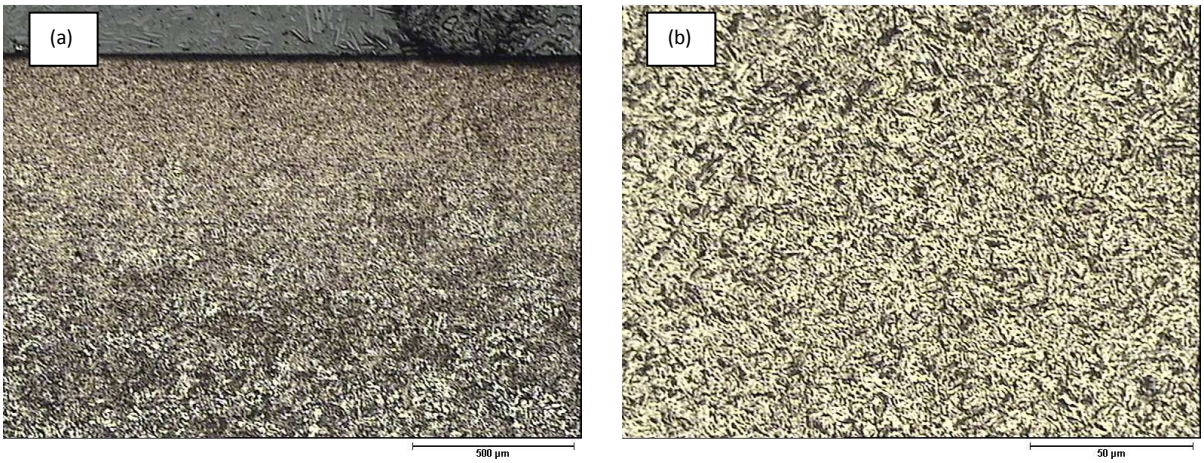

Figure 3 - Optical micrographs showing cross-sections of the steel pins in the cemented zone: (a) 50x, (b) 500x.

3.2 Pin-on-disk wear tests

Figures 4a and 4b depict the friction coefficient calculated by the equipment during the tests. When a 650 N normal load is applied in dry and wet conditions (Figure 4a), the friction coefficient shows many fluctuations around the average value. These fluctuations are associated with high frequency squeaky noise developed concurrently with the rise of friction coefficient and the metallic film deposition on the ceramic surfaces. Both curves follow the same pattern. At the beginning of each test the friction coefficients are quite low ($\mu \cong 0.1 \div 0.2$) and then progressively increase as the test proceeds. After about 2000 m, values reach a quasi steady-state ($\mu \cong 0.3 \div 0.4$). These values remain constant until the end of the tests. When a 450 N normal load is applied in dry condition (Figure 4b) the friction coefficient rises rapidly during the first few minutes and reach the quasi steady-state at only 500 m. The increasing of friction coefficient is due to the continuous generation of wear debris in the form of hard particles entrapped between the worn surfaces. Plastic deformation process during friction also increases hardness of these particles, so they scrape the surrounding material. When a 450 N normal load is applied in wet condition the tribological behaviour is very different. The friction coefficient remains constant at very low value ($\mu \cong 0.1$) until the sliding distance of 3000 m. Then rises slowly until it reaches the value of about $\mu \cong 0.2$ at the end of the test.

Figure 5a shows total wear when a 650 N normal load is applied, in dry and wet conditions. Also in this case, both curves follow the same pattern. Wear is negative up to a sliding distance of about 3500 m in dry conditions, then progressively increases as the test proceeds. At the end of the tests wear is positive and equal to 0.45 mm. In wet conditions wear reverses its trend for a sliding distance of about 2500 m and reaches at the end of the test approximately the same value as the previous case. When a 450 N normal load is applied in dry conditions (Figure 5b) the wear rises rapidly after about 2500 m up to the positive value of 0.29 mm. As for the friction coefficient, when a 450 N normal load is applied in wet conditions the tribological behaviour is very different. The total wear remains negative and gradually decreasing. Negative wear in Figure 5a for both wet and dry conditions and negative wear in Figure 5b only for a relative humidity of 15% indicate material build-up on the coating surface; this is caused by the formation of a thick oxide layer under condition of high surface temperatures (e.g. due to high load and sliding speed) and subsequent wear debris transfer from pin onto the disk. The oxide developed on the surface may be partially removed or retained as freely-moving particles between the contacting materials, acting as

three-body abradents. If the oxide layer is well-adherent to the metal substrate, it can continue to thicken and can reduce metal/ceramic contact, providing protection against wear damage [11]. The positive wear during the second part of the tests is due to fragmentation of tribolayer and to abrasion damage of coating surface. When a 650 N normal load is applied at the humidity of 95% wear reverses its trend for a sliding distance less than in dry conditions. The increasing of relative humidity reduces surface temperatures by water adsorption on ceramic coatings. In wet conditions the tribolayer is thinner than in dry condition, providing a less effective wear protection. As the test proceeds, the water desorption on Cr_2O_3 coating and the partially removal of oxide layer determine the progressive increase of total wear. When a 450 N normal load is applied in wet conditions (Figure 5b) the water adsorption on ceramic coating and the lower contact pressure prevent the increase of surface temperature. It is well-known that oxide surfaces adsorb water either dissociatively or molecularly. If water is dissociatively adsorbed many strongly bound surface hydroxyl groups are formed to the surface. The water desorption on Cr_2O_3 occurs above 500°C and leads to a surface structure, which cannot be recovered by rehydroxylation of the surface [28, 29]. In this case the surface temperature is widely lower than 500°C and the total wear remains negative for the duration of the test. Some authors also suggest that the reduction of the oxidation rate is due to the formation of iron hydroxide and ferri-oxide-hydrate [13, 14]. These oxides can act as protective layers preventing metal/ceramic interaction.

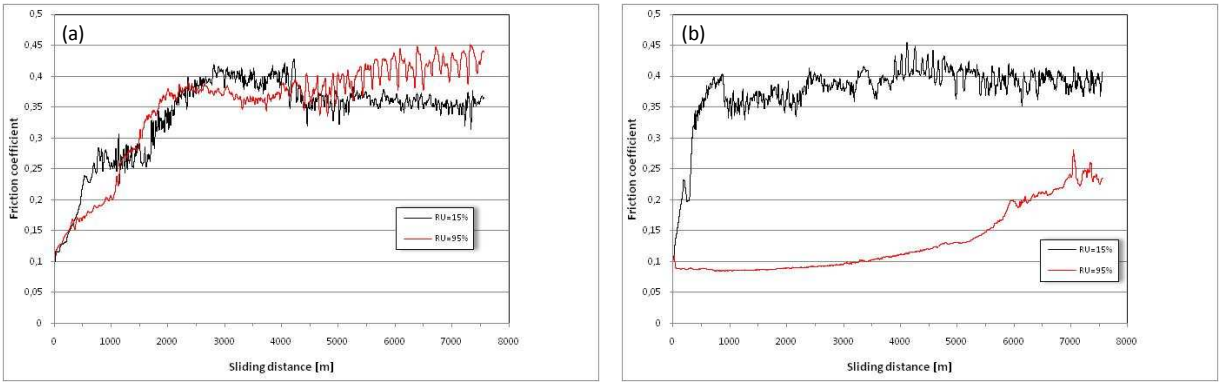

Figure 4 - Friction coefficient variation in different conditions for (a) 650 N and (b) 450 N normal loads.

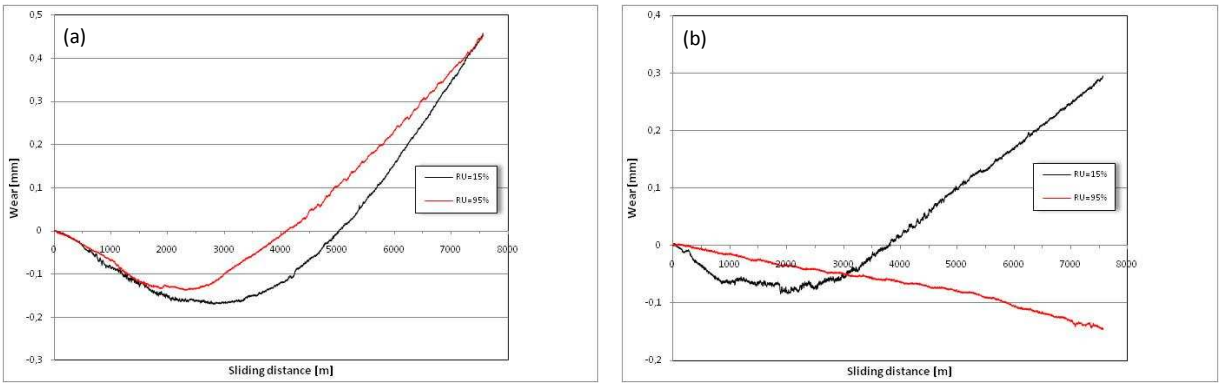

Figure 5 - The amount of wear in different conditions for (a) 650 N and (b) 450 N normal loads.

Figure 6a shows the wear scar profiles of the disks under different normal load and relative humidity conditions. It can be seen that the depth of wear track increases in the following order 450N_RU95% < 450N_RU15% < 650N_RU95% < 650N_RU15%. When a normal load of 450 N is applied in wet conditions, no wear damage is found and the wear scar profile (blue line in Figure 6a) is comparable with the roughness of the ceramic coating. In contrast, when the same load is applied in dry conditions, metallic film transfer occurs on the Cr_2O_3 coating due to localised melting of oxide interlayers. Correspondingly, isolated peaks are observed inside the wear track (green line in Figure 6a). When a 650 N normal load is applied in dry and wet conditions, a greater quantity of peaks inside the wear tracks is observed (red and black lines in Figure 6a). Moreover, some others peaks can be seen at the edges of the wear tracks. The sliding motion between metal and ceramic is accompanied by the formation of wear debris. Some of these particles are thrown out from the contact area and accumulated along the sides of the sliding tracks.

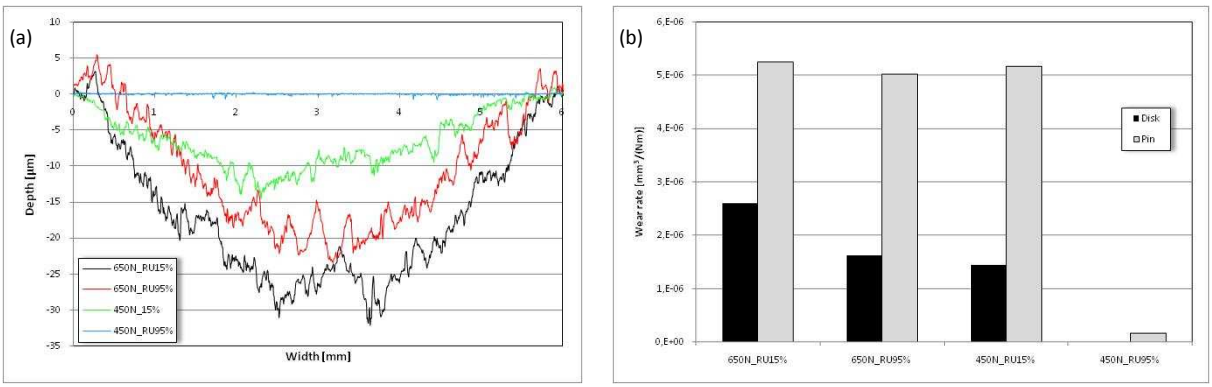

Figure 6 - (a) Wear scar profiles of the disks under different normal load and relative humidity conditions. (b) Wear rate of pins and disks under the same different conditions.

Figure 6b depicts the wear rate of pins and disks under the same different normal load and relative humidity conditions. In any case, the pin undergoes a significant loss of material. Except for a 450 N normal load applied in wet conditions, the wear rate is approximately 5 x 10^{-6} mm^3/(Nm). When a 450 N load is applied in wet conditions, the wear rate is six orders of magnitude lower than those for the other pins. Many studies concerning the tribological behaviour of high carbon steels in dry sliding suggested that if the wear rate is greater than 1 x 10^{-8} mm^3/(Nm), the wear can be considered as severe wear. Moreover, they found the greater wear rate corresponds to the higher friction temperature [30-33]. The wear rate of the disks decreases in the following order 650N_RU15% > 650N_RU95% > 450N_RU15%. However, when a 450 N normal load is applied in dry conditions, the wear rate is comparable with the value obtained when a 650 N normal load is applied in dry conditions. No wear rate is indicated for the disk when a 450 N normal load is applied in wet conditions, because the wear damage is three orders of magnitude lower than all the others.

The SEM micrographs of the coating worn surface, for a 650 N normal load applied in dry conditions, are shown in Figures 7a, 7b and 7c. It can be seen the material transfer from metallic pin onto the ceramic surface (Figure 7a). In particular, the wear scar with metallic film deposition could be divided into two zones. The first one is covered by a smooth iron oxide layer (Figure 7b). It is in good agreement with previous studies, which show that, if the thermal conductivity of a material is not sufficiently high, the surface temperature can exceed melting temperature. Consequently, the melting of local areas on the worn surfaces and in the subsurface layers can be observed. Some works indicate localised melting occurs not only at higher normal loads and sliding speeds, but even at sliding speeds as modest as 1 m/s [20, 33, 34]. Metallic film is firmly attached to the Cr_2O_3 coating, because of the strong adhesion between the sliding surfaces: it is plastically deformed and oriented in the direction of the sliding motion. Scratches and local plastic deformations are indicated in Figure 7b. This adhesive metal transfer justifies the peculiar pattern of the ceramic wear scar profile observed in Figure 6a. In the second zone, many pits are uniformly distributed over the wear track (Figure 7c): wear debris in the form of flakes is also generated. During sliding in dry conditions, microcracks and dislocation networks can produce fine wear debris as observed in the worn surface. Some wear particles are entrapped in the contact interface and subjected to continued fracture, deformation or chemical reaction, producing microsized powders. It can be demonstrated that at higher loads, wear debris can not be taken away and the amount of

wear particles deposited on the worn surface increases with normal load applied. Moreover, smooth oxide layers are bigger and scratches are deeper in higher loading conditions [23, 35].

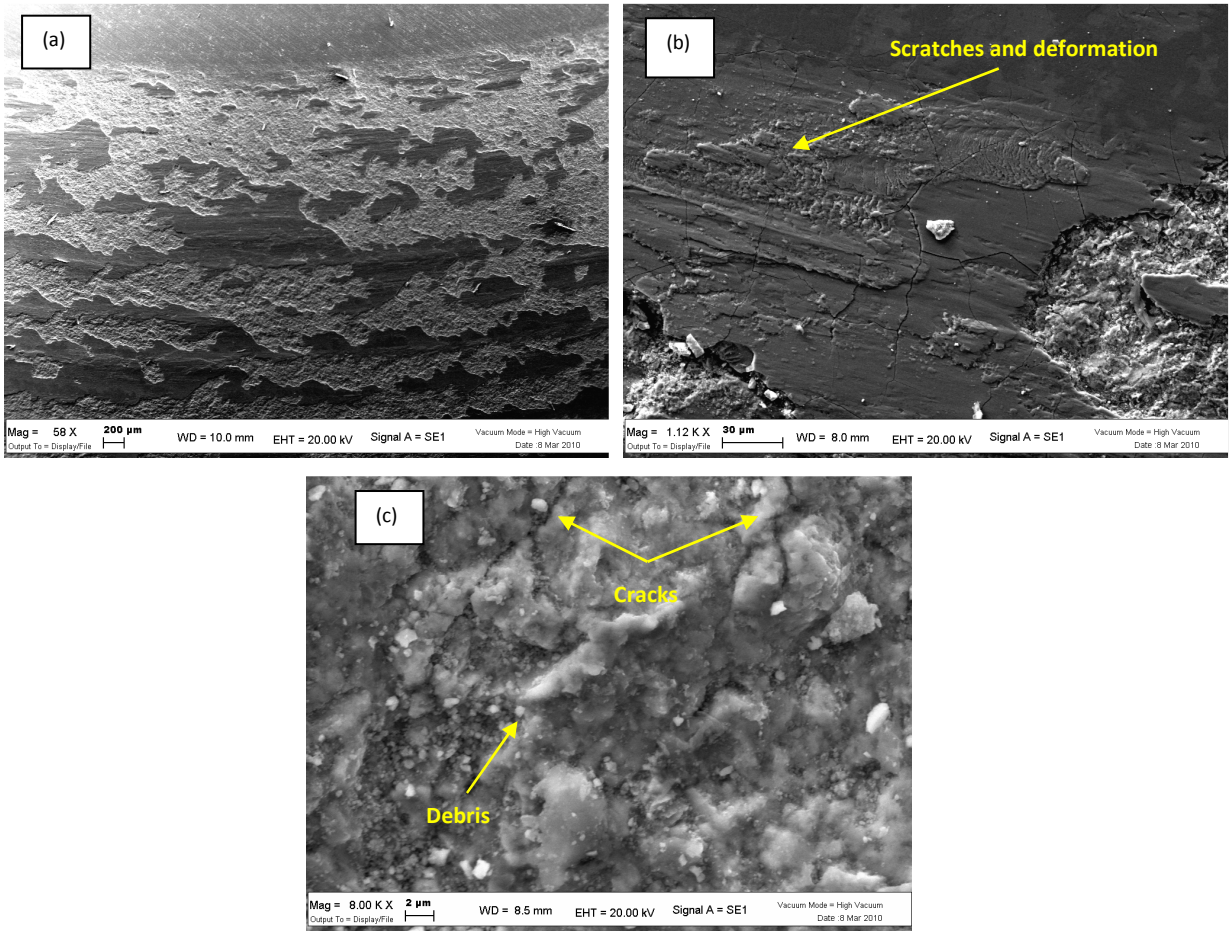

Figure 7 - SEM micrographs of the Cr_2O_3 worn surface for a 650 N normal load applied in dry condition: (a) overview of the wear scar, (b) detail of the metallic film transfer, (c) details of cracks and wear debris.

Figure 8 shows the SEM micrograph of the worn coating surface and corresponding EDS analyses results, when a 650 N normal load is applied in dry conditions. EDS analysis on the metallic film indicates the presence of a great amount of iron and traces of other alloying elements such as chromium and nickel, transferred onto the ceramic coating. In contrast, EDS analysis of the original ceramic surface indicates the presence of a great amount of chromium and traces of iron as wear particles. A subsequent X-ray diffractometry examination enabled the type of film to be distinguished (Figure 9). It is a Fe_2O_3 compound, which generally forms when the contact temperature rises over about 200 °C. A comparison between Figure 9 and Figure 2 shows that Cr_2O_3 coating does not change its chemical composition after the wear test.

When a 650 N normal load is applied in wet conditions and for a 450 N normal load applied in dry conditions (Figure 10), the morphology of the coating worn surfaces and the wear mechanisms are similar to the previous case. The SEM micrograph in Figure 10a depicts an overview of the wear scar. The amount of smooth oxide layers can be compared to metal transfer observed in Figure 7a, but scratches are shallow. Figure 10b shows the details of fracture on the original ceramic surface. In agreement with the microstructure of the coating, it can be seen that microfractures develop along the columnar grains in perpendicular direction to the surface and along splat boundaries since their strength usually is not high enough. At higher magnification, pits are also visible (Figure 10c).

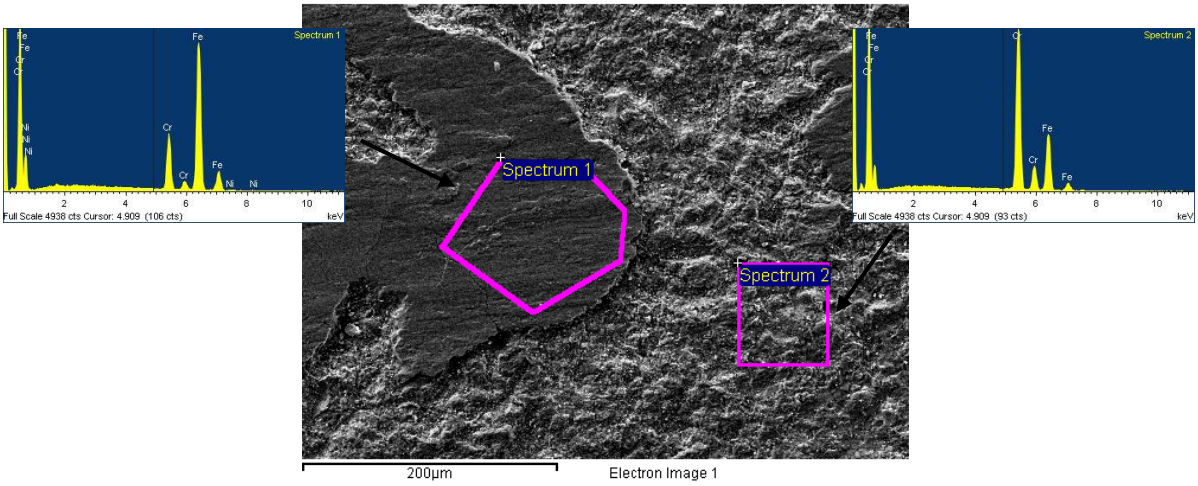

Figure 8 - SEM micrograph and EDS analyses' results of Cr_2O_3 worn surface, when a 650 N normal load is applied in dry conditions.

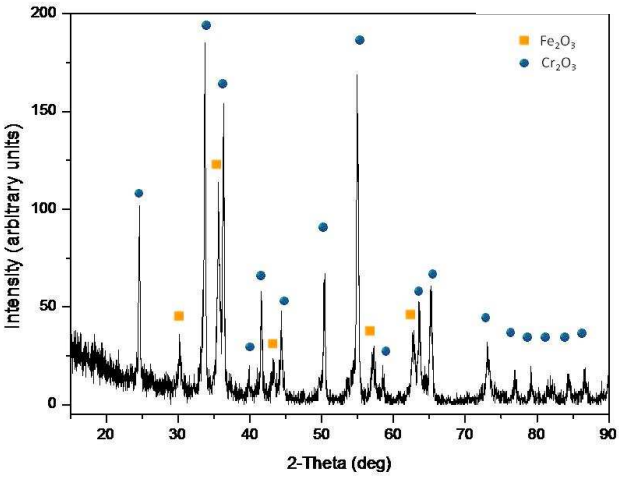

Figure 9 - XRD pattern of Cr_2O_3 worn surface for a 650 N normal load applied in dry condition.

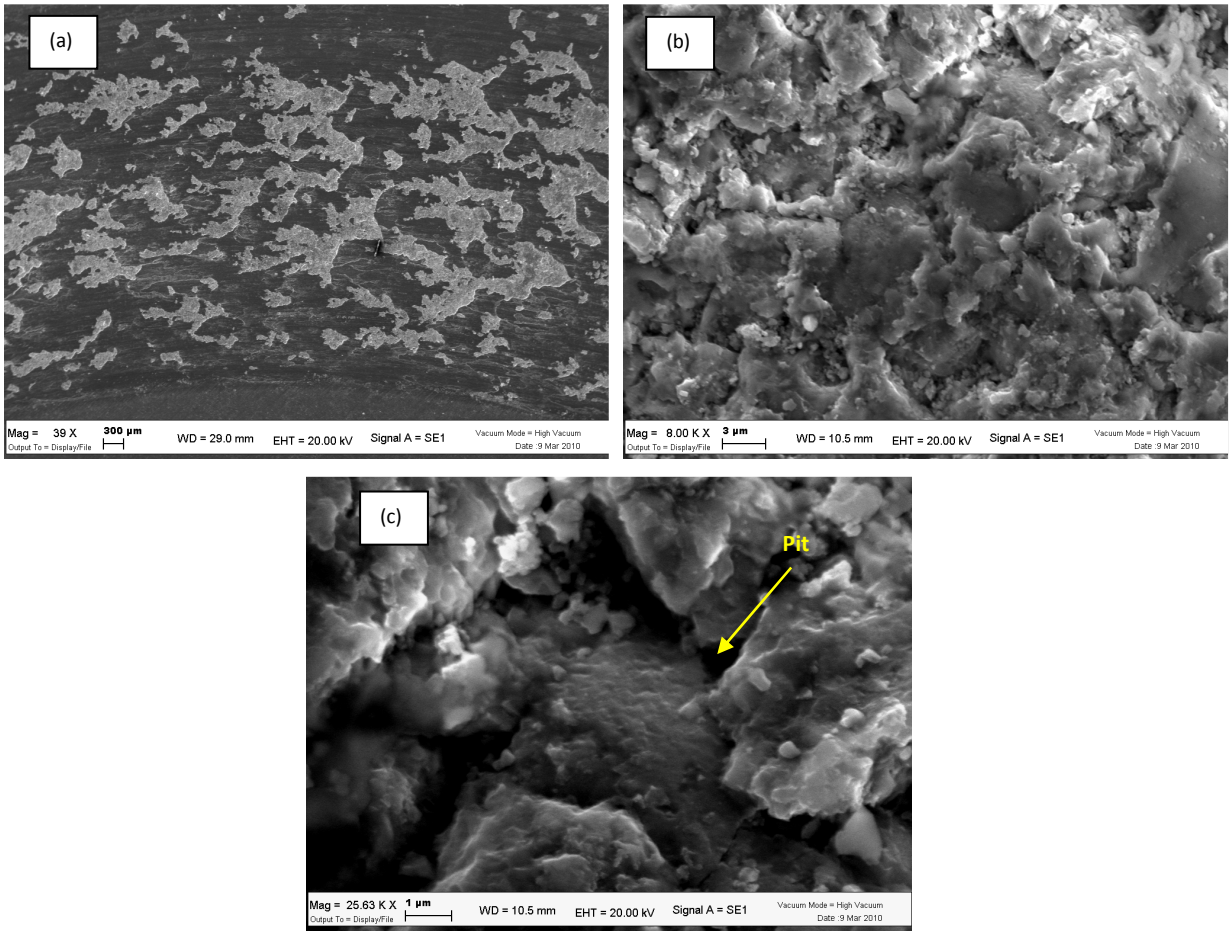

Figure 10 - SEM micrographs of Cr_2O_3 worn surface, when a 450 N normal load applied in dry condition: (a) overview of the wear scar, (b) detail of cracks and wear debris, (c) detail of a pit.

When a 450 N normal load is applied in wet conditions, no wear damage is observed on the ceramic coating (Figure 11a). The surface appears smoother without evidence of significant wear and pores remain open in the flattened surface (Figure 11b).

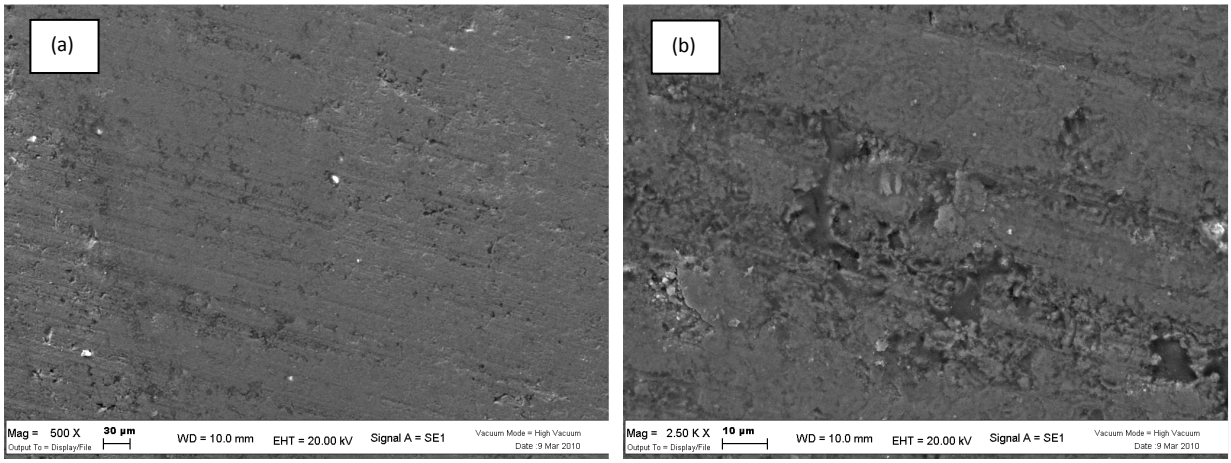

Figure 11 - SEM micrographs of Cr_2O_3 worn surface for a 450 N normal load applied in wet condition: (a) overview of the wear scar, (b) detail of open porosity.

The SEM micrographs of a pin worn surface for a 650 N normal load applied in dry conditions and when a 450 N normal load is applied in wet conditions are shown in Figure 12a and 12b, respectively. In the first case (Figure 12a), the surface is very rough and plastically deformed with the ploughing appearance typical of adhesive wear. A thick film of iron oxide covers the worn surface with a mainly dark grey colour as revealed by optical microscopic observations (Figure 13). The metallic film is discontinuous, indicating the wear mechanism involves both the removal and re-formation of the oxide film and wear of free metallic surface. Many studies suggest that, in the mild-oxidational wear regime, oxidation is caused by frictional heat. The oxide film grows until it reaches a critical thickness (about 10 μm for steel), then it spalls off as wear debris. For high normal loads and sliding speeds a transition to severe-oxidational wear can occurs. This is associated with the localised melting of the oxide layer to a viscous liquid that can flow under the sliding action. At this time, the melt-dominated wear replaces adhesion and delamination-dominated mechanisms [10, 11, 31-33]. When a 650 N normal load is applied in wet conditions and for a 450 N normal load applied in dry conditions, the morphology of the pin worn surfaces and the wear mechanisms are similar to the previous case. When a 450 N normal load is applied in wet conditions, no significant wear damage is observed (Figure 12b). Only a little amount of metallic oxide appears on the pin worn surface. Moreover, the working marks are still visible.

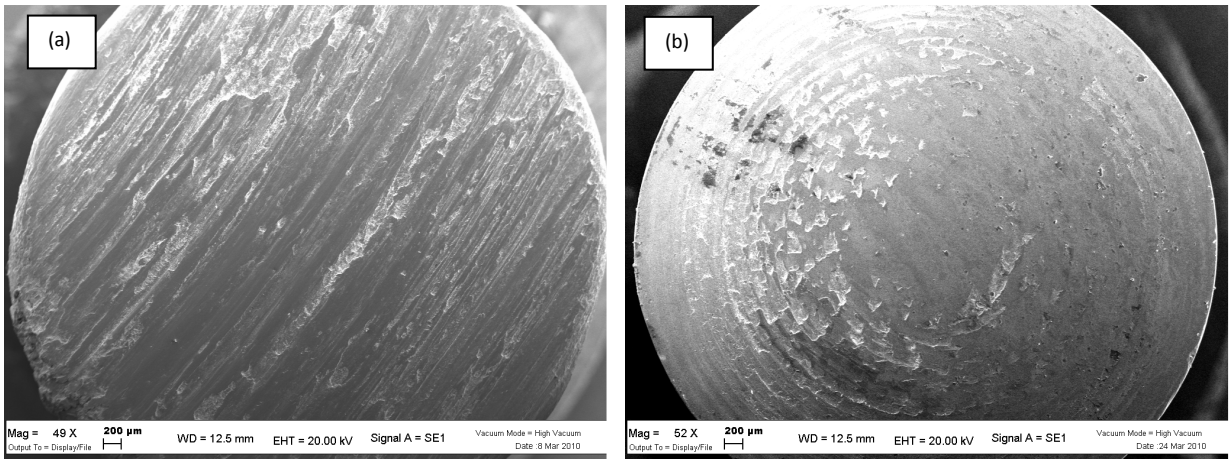

Figure 12 - SEM micrographs of pins worn surface: (a) for a 650 N normal load applied in dry conditions, (b) when a 450 N normal load is applied in wet conditions.

For a 650 N normal load applied in dry conditions, optical microscope observations of the pin cross-sections can provide information about the dynamic changes in worn surface layers (Figure 13). The sliding wear between metal and ceramic surfaces results in a laminated

structure. In particular, it consists of an about 10 μm-thick iron oxide layer (A); a layer of a very fine structure without a defined position and orientation (B); a fine structure with a clearly defined position and orientation (C); a plastically deformed layer (D) and the unaffected structure (E). It is well-known that, for a given material, the characteristic structural layers appear depending upon test conditions. In general, the thickness of the plastically deformed layer is related to the properties of material itself. Structures with low plasticity and low thermal conductivity (e.g. martensite) are difficult to deform. It results in a higher surface temperature and a thinner plastically deformed layer. In contrast, structures with good plasticity and high thermal conductivity (e.g. pearlite) are easier to deform and less heat accumulates at surface. Accordingly, a thicker plastically deformed layer can form. The morphology of the material build-up, accumulated at the edge of the pin worn surface, is observed in Figure 14a. It is plastically deformed due to the sliding motion and the highest surface temperature. It also consists of a very fine sorbitic microstructure with a great amount of carbides uniformly distributed (Figure 14b). Optical microscope examinations of the pins' cross-sections, for a 450 N normal load applied in wet conditions, show the same microstructure found before the wear test (Figure 15). No evidence of a laminated structure and of the material build-up, accumulated at the edge of the pin worn surface, are observed.

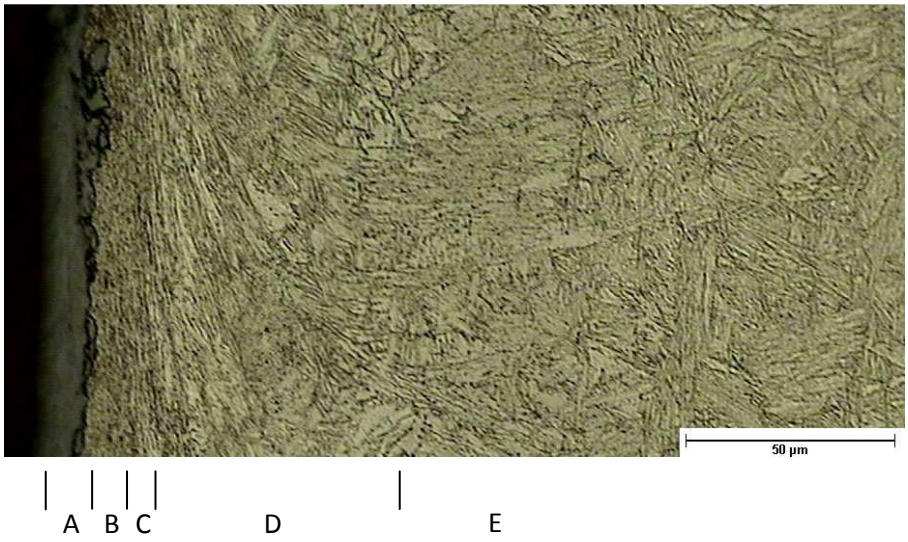

Figure 13 - Optical micrographs of a pin worn surface, when a 650 N normal load is applied in dry conditions.

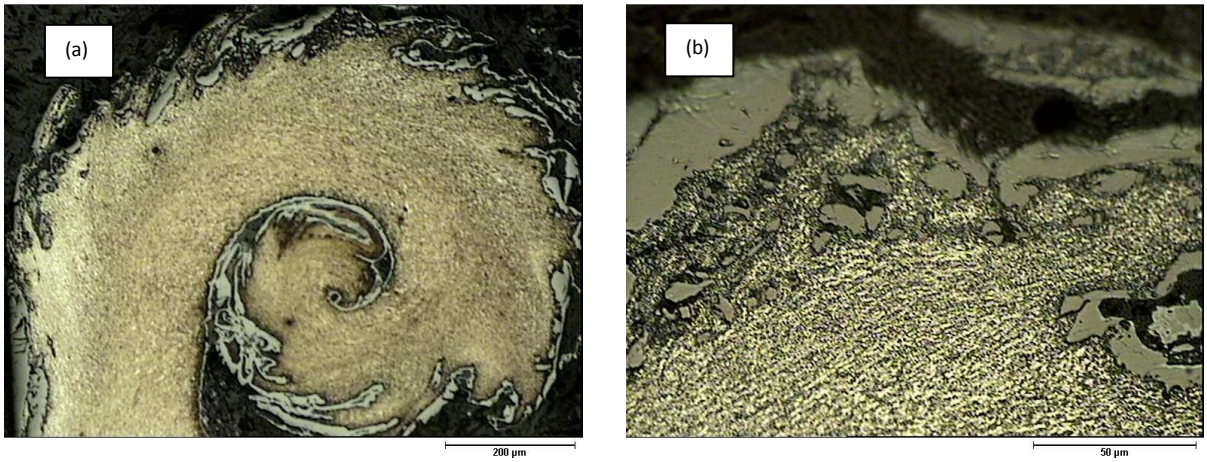

Figure 14 - Optical micrographs of a pin worn surface, when a 650 N normal load is applied in dry conditions: (a) detail and (b) microstructure of the material build-up at the edge of the sliding surface.

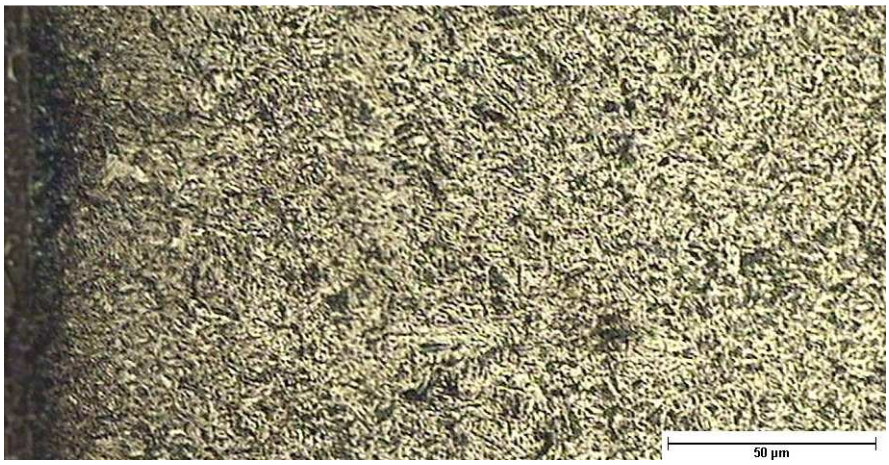

Figure 15 - Optical micrographs of a pin worn surface, when a 450 N normal load is applied in wet conditions.

Figure 16a shows the microhardness profiles of the pin worn surfaces, when a 650 N normal load is applied in different conditions. It can be seen there is a very narrow region just below the worn surface with high microhardness. Both curves rapidly decrease and reach values comparable to the microhardness of the base un-cemented material. During sliding wear, friction energy is used to produce plastic deformation and heat. Strain gradient and temperature gradient in worn surface layers affect the hardness distribution. Many internal factors affect the hardness of worn surface layers of a steel, such as strain hardening, recovery and recrystallization, precipitation hardening, thermal martensitic transformation tempering and so on. Therefore, the hardness profiles measured after wear tests reflect the competition between the factors that cause hardening and those that cause softening. It can be also demonstrated that a originally softer microstructure, which has a higher value of the work

hardening coefficient (e.g. pearlite), is likely to show hardening. An originally harder microstructure, which has a lower value of the work hardening coefficient (e.g. martensite), is likely to show softening. This is in accordance with drop of the microhardness profile observed in Figure 16a. The wear volume is also related to the hardening and softening behaviour resulting from dynamic changes in worn surface layers. Generally, a smaller softening response corresponds to a better wear resistance [31-33]. When a 450 N normal load is applied in dry conditions the softening trend of surface layers is the same as the previous cases (Figure 16b). For a 450 N normal load applied in wet conditions, the microhardness profile is typical of a steel subjected to an hardening surface treatment. There is no evidence of strain hardening or softening due to the sliding wear.

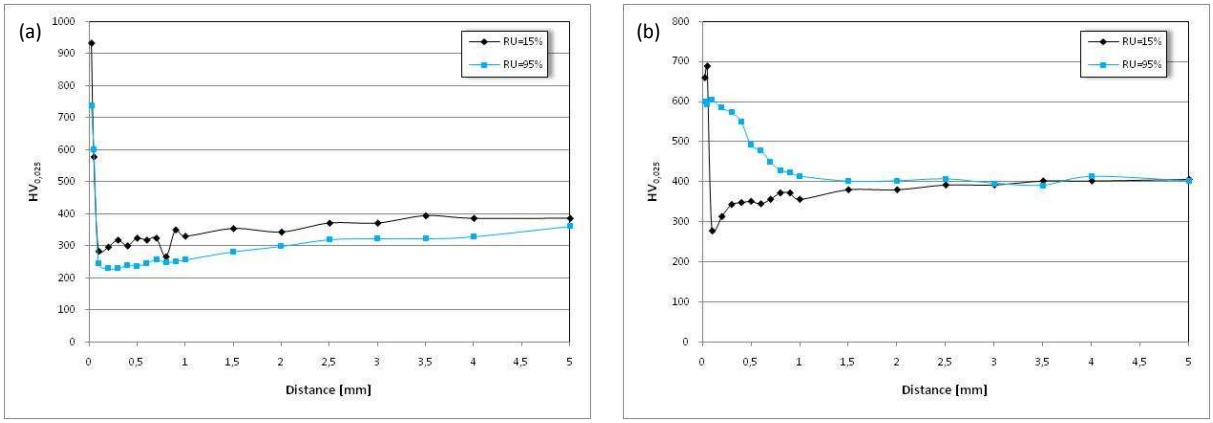

Figure 16 - Microhardness profiles of the pins' worn surfaces when: (a) a 650 N and (b) a 450 N normal load are applied in different humidity conditions.

4. CONCLUSIONS

Based on the results obtained regarding friction and wear behaviour of a carbon steel in sliding contact with a Cr_2O_3 plasma-sprayed ceramic coating, the following conclusions can be drawn:

- In dry and wet conditions, wear rates of the ceramic coating decrease with normal load. In dry conditions, wear rates of pins are independent of the normal loads applied. For a lower normal load applied in wet conditions, the wear rate of pins is reduced of about six orders of magnitude.

- For all the normal loads applied in dry conditions, metal/ceramic sliding contact produces a metallic film transfer onto the ceramic surface. Metallic film consists of a Fe_2O_3 compound usually formed at temperatures over about 200 °C. The presence of this oxide suggests a progressive increase in the contact temperatures as wear tests proceed. The observations of pins' worn surfaces indicate that the principal involved wear mechanism is the mild-oxidational wear, with ploughing and a plastic deformation appearance. The dynamic changes in the surface layers of the material also result in a laminated structure. The subsequent transition to severe-oxidational wear is associated with the localised melting of the oxide layer and its spreading on the ceramic surface. As concern the ceramic coating, the observations of Cr_2O_3 worn surfaces indicate it undergoes microfractures along splat and columnar grains boundaries.

- In wet conditions, the normal load applied influences the tribological behaviour of metal/ceramic sliding couplings. For the highest normal load the wear mechanisms are the same involved in dry conditions. For the lower normal load the reduction of the surface temperatures, and consequently of the oxidation rate, is due to the water adsorption on the worn surfaces. The moisture adsorbed can act as a protective layer preventing metal/ceramic interaction.

ACKNOWLEDGEMENTS

The authors would like to thank Zocca Officine Meccaniche (Funo, BO) for the thermally sprayed coating manufacturing, and Ing. Marco Vitali for the contribution to the experimental activity.

REFERENCES

[1] H.A. Bolton, J.M. Larson, Valvetrain system design and materials, ASM International, Materials Park, OH, (2002).

[2] C.T. Sims, N.S. Stolloff, W.C. Hagel, Superalloys II: high temperature materials for aerospace and industrial power, Wiley- Interscience, New York, (1987).

[3] M.J. Donachie, S.J. Donachie, Superalloys - a technical guide, 2nd edn., ASM International, Materials Park, OH, (2002).

[4] F.H. Stott, D.S. Lin, G.C. Wood, 'Glazes' produced on nickel-based alloys during high temperature wear, Nature 242 (1973) 75-77.

[5] F.H. Stott, D.S. Lin, G.C. Wood, Structure and mechanism of formation of the 'glaze' oxide layers produced on Ni-based alloys during wear at high temperatures, Corrosion Science 13 (66) (1973) 449-469.

[6] P.J. Blau, T.M. Brummett, B.A. Pint, Effects of prior damage on high-temperature oxidation of Fe-, Ni-, and Co-based alloys, Wear 267 (2009) 380-386.

[7] F.H. Stott, G.C. Wood, The influence of oxides on the friction and wear of alloys, Tribology International 11 (4) (1978) 211-218.

[8] T.F.J. Quinn, Review of oxidational wear Part I: The origins of oxidational wear, Tribology International 16 (5) (1983) 257-271.

[9] S.C. Lim, M.F. Ashby, Overview no. 55 Wear-mechanism maps, Acta Metallurgica 35 (1) (1987) 1-24.

[10] F.H. Stott, High-temperature sliding wear of metals, Tribology International 35 (2002) 489-495.

[11] F.H. Stott, The role of oxidation in the wear of alloys, Tribology International 31 (1-3) (1998) 61-71.

[12] P.J. Blau, Elevated-temperature tribology of metallic materials, Tribology International 43 (2010) 1203-1208.

[13] W.Y.H. Liew, Effect of relative humidity on the unlubricated wear of metals, Wear 260 (2006) 720-727.

[14] P. De Baets, G. Kalacska, K. Strijckmans, F. Van De Velde, A.P. Van Peteghem, Experimental study by means of thins layer activation of humidity influence on the fretting wear of steel surface, Wear 216 (1998) 131-137.

[15] H. Goto, D.H. Buckley, The influence of water vapour in air on the friction behaviour of pure metals during fretting, Tribology International 18 (4) (1985) 237-245.

[16] G. Bregliozzi, S.I.-U. Ahmed, A. Di Schino, J.M. Kenny, H. Haefke, Friction and wear behaviour of austenite stainless steel: influence of atmospheric humidity, load range and grain size, Tribology Letters 17 (2004) 697-704.

[17] E. Tsuji, A. Ando, Effects of air and temperature on speed dependency of sliding wear of steel, JSLE ASLE International Lubrication Conference, Tokyo (1975) 101-109.

[18] S. Asanabe, Applications of ceramics for tribological components, Tribology International 20 (1987) 355-364.

[19] V. Aronov, T. Mesyef, Wear in ceramic/ceramic and ceramic/metal reciprocating sliding contact. Part1, ASME/ASLE Joint Tribology Conference, Atlanta (1985) 16-21.

[20] G.W. Stachowiak, G.B. Stachowiak, A.W. Batchelor, Metallic film transfer during metal-ceramic unlubricated sliding, Wear 132 (1989) 361-381.

[21] B. Wang, Z.R. Shui, A.V. Levy, Sliding wear of thermal-sprayed chromia coatings, Wear 138 (1990) 93-110.

[22] A. Tronche, P. Fauchais, Frictional behaviour against steel of aluminium substrates plasma-sprayed with hard coatings, Materials Science and Engineering: A 102 (1988) 1-12

[23] H. Cetinel, E. Celik, M.I. Kusoglu, Tribological behaviour of Cr_2O_3 coatings as bearing materials, Journal of Materials Processing Technology 196 (2008) 259-265.

[24] J.E. Fernandez, Y. Wang, R. Tucho, M.A. Martin-Luengo, R. Gancedo, A. Rincón, Friction and wear behaviour of plasma-sprayed Cr_2O_3 coatings against steel in a wide range of sliding velocities and normal loads, Tribology International 29 (4) (1996) 333-343.

[25] C.B. Ponton, R.D. Rawlings, Vickers indentation fracture toughness test. Part 1: Review of literature and formulation of standardised indentation toughness equations, Materials Science and Technology 5 (1989) 865-872.

[26] C.B. Ponton, R.D. Rawlings, Vickers indentation fracture toughness test. Part 2: Application and critical evaluation of standardised indentation toughness equations, Materials Science and Technology 5 (1989) 961-976.

[27] G. Bolelli, V. Cannillo, L. Lusvarghi, T. Manfredini, Wear behaviour of thermally sprayed ceramic oxide coatings, Wear 261 (2006) 1298-1315.

[28] S. Kittaka, K. Morishige, J. Nishiyama, T. Morimoto, The effect of surface hydroxyls of Cr_2O_3 on the adsorption of N_2, Ar, Kr, and H_2O in connection with the two-dimensional condensation, Journal of Colloid and Interface Science 91 (1) (1983) 117-124.

[29] M. Harju, T. Mäntylä, K. Vähä-Heikkilä, V. Lehto, Water adsorption on plasma sprayed transition metal oxides, Applied Surface Science 249 (2005) 115-126.

[30] E. Takeuchi, Friction and wear of machine parts - Surface heat treatments for increase wear resistance, Machine Tools 23 (5) (1979) 68-74.

[31] Y. Wang, T. Lei, J. Liu, Tribo-metallographic behaviour high carbon steels in dry sliding I. Wear mechanisms and their transition, Wear 231 (1999) 1-11.

[32] Y. Wang, T. Lei, J. Liu, Tribo-metallographic behaviour high carbon steels in dry sliding II. Microstructure and wear, Wear 231 (1999) 12-19.

[33] Y. Wang, T. Lei, J. Liu, Tribo-metallographic behaviour high carbon steels in dry sliding III. Dynamic microstructural changes and wear, Wear 231 (1999) 20-37.

[34] X.D. Li, Y. Wang, J.J. Liu, A study on dry friction of eutectoid steel, Wear 150 (1991) 59-65.

[35] H.S. Ahn, O.K. Kwon, Tribological behaviour of plasma-sprayed chromium oxide coating, Wear 225-229 (1999) 814-824.

Article 3

FRICTION AND WEAR BEHAVIOUR OF APS AND HVOF ADVANCED CERAMIC COATINGS

COMPORTAMENTO TRIBOLOGICO DI RIVESTIMENTI CERAMICI AVANZATI APPLICATI MEDIANTE TECNICHE APS E HVOF

Mattia Merlin, Chiara Soffritti, Reyna Vazquez, Gian Luca Garagnani

Department of Engineering - ENDIF
University of Ferrara
I-44122 Ferrara
Italy

Proceedings of 33° Convegno Nazionale AIM, Brescia, Italy, November 10-12, 2010

ABSTRACT

In this paper is reported a research activity carried out in order to evaluate the tribological behaviour of four types of advanced ceramic coatings, Al_2O_3-13TiO_2, Cr_2O_3, WC-12Co and Cr_3C_2-37WC-18Me, deposited onto cemented steel plates. The ceramic coatings are applied by plasma-spraying (APS), while the cermet coatings are deposited by HVOF-spraying technique. Pin-on-disk wear tests are performed by means of a DUCOM tribometer in accordance with ASTM G99-05 standard, using alumina pins as counterpart material. The tests are carried out under different conditions of relative humidity; other test parameters, such as normal load, test duration, sliding speed and temperature, are maintained constant. Optical Microscope (OM) and Scanning Electron Microscope (SEM) observations of the worn surfaces show the interaction of different wear mechanisms, confirming the importance of relative humidity in relation to the nature of the coatings employed.

KEYWORDS: Sliding wear; Thermal spraying; Advanced ceramic coatings; Relative humidity

1. INTRODUCTION

Ceramic and cermet coatings are widely used in industrial applications that require friction and wear resistance due to their high hardness, chemical stability, oxidation-resistance at high temperatures and thermal barrier properties [1]. However, their brittle character and high cost of production restrict the applications of bulk ceramics in industry to a certain extent. For this reason, ceramic and cermet coatings deposited onto materials which are cheap and reliable in shock, such as steels, are more frequently employed. The advanced ceramic coatings have already found engineering applications as tribological components, e.g. in water pumps, cylinders drying for paper mills, rolling bearings and valves [2-7].

Compared to traditional coating manufacturing techniques, thermal spraying is considered a potential alternative for the production of wear-resistant coatings. A large variety of hard materials, including ceramics and cermets, can be deposited onto many types of substrate in order to obtain very hard coatings, preventing thermal alteration of the substrate. Consequently, they are used in all cases when design tolerances must be satisfied, when thin-walled components must be considered or when heat-sensitive materials (like Al and Mg alloys) need to be processed. In general, a thermal-sprayed coating is obtained by using feedstock in the form of micro or nano-size particles which are melted (or heated) by electrical or chemical means and ejected with variable temperature and speed. The molten droplets are subsequently projected onto the substrate that needs to be coated. Compared to the bulk of material, the presence of defects, e.g. porosity, oxide lamellas and unmolten particles, can reduce the tribological performance of the coating. Moreover, the coating-substrate low adhesion that normally characterises the thermal-sprayed coatings, limits their technological applications. Accordingly, in the last decade an intensive research activity is aimed at evaluating the influence of these typical defects on the quality of advanced ceramic coatings.

Plasma-spraying (APS) and HVOF-spraying are the thermal spraying techniques most commonly used to obtain high quality wear-resistance coatings. HVOF is developed to overcome the limitations of plasma-spraying: it is well-known that HVOF-spraying, if used for the production of cermet coatings, is more effective than plasma-spraying, because of the highest gas jet velocity and lowest flame temperature that result in coatings with low splat oxidation, low porosity and low carbide decomposition and/or dissolution [8-11]. However, the limitations of HVOF are mainly related to the cost of powders, the difficulty of preparing and the limited availability of commercial torches. Thus, plasma-spraying is still the most

widely employed production technique for ceramic coatings, like Al_2O_3 and Cr_2O_3. Such coatings are more porous and brittle than cermet coatings obtained by HVOF, because of intrinsic porosity due to lower particles in-flight velocity [12-15]. However, they possess high hardness, low susceptibility to many corrosive environments and they can stand at high temperatures.

The study of the tribological behaviour of plasma-spraying and HVOF-spraying coatings is fundamental for their correct employment in many applications, even when the environmental humidity is critical for a proper operating of the tribological system [2, 3]. In the research activity reported in this paper, four types of advanced ceramic coatings, Al_2O_3-$13TiO_2$, Cr_2O_3, WC-12Co and Cr_3C_2-37WC-18Me, are deposited onto cemented steel plates. The ceramic coatings are applied by plasma-spraying, while the cermet coatings are deposited by HVOF-spraying technique. The aim of this work is to study the wear resistance of these coatings, through pin-on-disk tests carried out under an applied normal load of 50 N and under two different conditions of relative humidity (20% and 70%). In particular, it is observed that the latter parameter greatly affects the tribological behaviour of the investigated ceramic and cermet coatings.

2. MATERIALS AND EXPERIMENTAL DETAILS

Four types of coating, namely Al_2O_3-$13TiO_2$ (powder: FST C-335.23, -45 +15 μm), Cr_2O_3 (powder: AMPERIT® 707.001, -45 +22.5 μm), WC-12Co (powder: WOKA 3102, -45 +15 μm) and Cr_3C_2-37WC-18Me (powder: WOKA 7505, -38 +10 μm), were deposited onto cemented steel plates (80 mm in diameter and 6 mm in thickness). A bond coat Ni-20%Cr was applied between the steel substrate and the ceramic coating, in order to improve adhesion. Chemical composition of the steel substrate was evaluated by Optical Emission Spectroscopy (OES) and the main results are collected in Table I.

Table I - Chemical composition (wt.%) of the steel substrate.

C	S	Mn	P	Si	Cr	Ni	Mo	Cu	V	Fe
0.22	0.033	0.88	0.021	0.30	0.84	0.87	0.06	0.202	0.022	bal.

The coatings were characterised by Vickers microhardness measurements (300 g_f load and 15 s loading time) carried out by means of a Microhardness Tester FM Future-Tech. Roughness

parameters (R_a and R_z) were calculated by the portable Handysurf E35_A ZEISS-TSK rugosimeter. Before each measurement all the coating surfaces are cleaned by ultrasonic bath. The LEICA MEF4M optical microscope, equipped with Archive4Images v.3.20b software for image analysis, was also employed on properly polished cross-sections to analyse the coatings microstructure. Image-Pro Plus v6.0 software was used in order to quantify coating porosity.
Pin-on-disk dry sliding tests were carried out with a Multispecimen Tester tribometer produced by DUCOM Instruments, in accordance with ASTM G99-05 "Standard test method for wear testing with a pin-on-disk apparatus", using cylindrical alumina pins of 6 mm in diameter and 22 mm in height as counterpart material. Normal load (5÷1000 N), sliding speed (20÷1400 rpm), temperature (≤ 200°C), relative humidity (0÷100%), test duration and total wear were continuously monitored during the tests. For each test, an applied normal load of 50 N, a sliding speed of 100 rpm and a test duration of 1 h were maintained constant, whereas the values of 20% and 70% of relative humidity were selected. Moreover, a mean of 10 tests for each coating were performed to verify the results. Wear rate of disks was evaluated by measuring the area of the wear track cross-section by an Optacom VC-10 profilometer. Each area, obtained as an average value of four measurements along the wear circumference, was used to calculate the wear volume. In order to understand wear mechanisms the coating worn surfaces were investigated by means of Optical Microscope (OM), and Scanning Electron Microscope (SEM).

3. RESULTS AND DISCUSSIONS

3.1 Microstructure and mechanical properties

Optical micrographs in Figure 1 show the microstructure of the four examined coatings. The Al_2O_3-13TiO_2 possesses a lamellar microstructure characterized by the presence of titania lamellae well-melted and partially mixed with alumina (Figure 1a). Moreover, pores and coarse particles can be seen at the steel/bond coat interfaces; these residues are probably resulting from the sandblasting process, normally performed before thermal spraying in order to improve the coating/substrate adhesion. As concern the Cr_2O_3 coating, also the optical micrograph in Figure 1b depicts a lamellar microstructure typical of coatings produced by plasma spray technique. Microstructure of both WC-12Co and Cr_3C_2-37WC-18Me coatings (Figure 1c and Figure 1d, respectively), consists of carbide particles embedded into a metallic matrix; at higher magnifications the carbides appear non-uniformly distributed and variable in

size, generally in the range of 1÷10 μm. Moreover, for WC-12Co coating, microcracks developed in parallel direction to the coating surface generate interconnecting porosity.

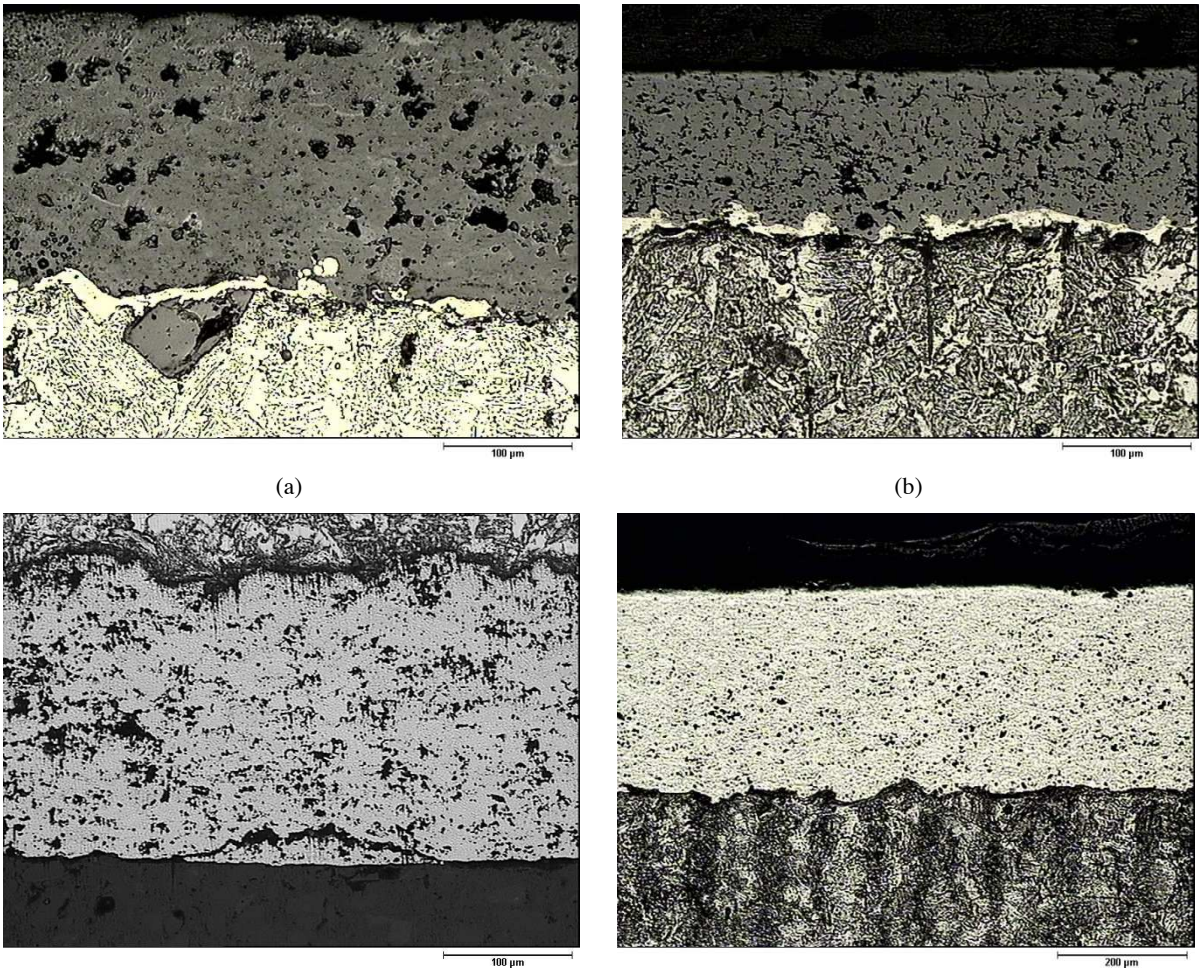

(a) (b)

(c) (d)

Figure 1 - Optical micrographs of the examined coatings: (a) Al_2O_3-13TiO_2, (b) Cr_2O_3, (c) WC-12Co, (d) Cr_3C_2-37WC-18Me.

The mechanical properties of each coating are investigated by Vickers microhardness and roughness measurements; in addition, the porosity is evaluated by image analysis performed by Image-Pro Plus v6.0 software. The main results are collected in Table II.

Table II - Mechanical properties, roughness and porosity of the employed materials.

	$HV_{0.3}$	R_a [μm]	R_z [μm]	Porosity [%]
Al_2O_3-13TiO_2	778 ± 53	0.25 ± 0.01	2.66 ± 0.23	13.7
Cr_2O_3	1188 ± 45	0.15 ± 0.02	1.78 ± 0.19	10.8
WC-12Co	1076 ± 186	0.35 ± 0.04	2.65 ± 0.27	14.7
Cr_3C_2-37WC-18Me	1181 ± 260	0.41 ± 0.03	2.93 ± 0.21	9.2
Pin	1500÷1650	-----	-----	-----

3.2 Tribological behaviour

The wear tests highlight the influence of relative humidity on the tribological behaviour of the examined advanced ceramic coatings. In Figure 2 are reported the mean values of the friction coefficient calculated at the end of the wear tests. For Cr_2O_3 and Cr_3C_2-37WC-18Me coatings the friction coefficient decreases as the relative humidity increases. In both cases, this behaviour can be attributed to the boundary lubrication due to water adsorption on coating surfaces; the "lubricant" is interposed between the coupling surfaces, reducing friction and wear [16]. The wear tests also suggest that the Cr_2O_3 is more sensitive to water adsorption. Friction coefficients obtained for the WC-Co coating are comparable for both values of the relative humidity. It is caused by two opposing phenomena: at low relative humidity the generation of a protective tribolayer, acting as solid lubricant, greatly reduces the friction coefficient. At high relative humidity the tribolayer is less adherent to the substrate; consequently, the predominant mechanism is the water adsorption [8, 17].

The tribological behaviour of Al_2O_3-13TiO_2 coating is very different: the friction coefficient increases as the relative humidity increases. The lower microhardness (see Table II in section 3.1) and the presence of an alumina-titania glassy phase weakens the ceramic material. Moreover, this coating does not form an adequately compact tribolayer and therefore shows unfavourable properties in terms of friction coefficient and wear rate (see Figure 4) [7].

Figure 3 shows an example of a wear scar profile of the Al_2O_3-13TiO_2 coating. The profiles are used to measure the area of the wear track cross-section; each area, obtained as an average value of four measurements along the wear circumference, is then employed to calculate the wear volume by the following relation, suggested by ASTM G99-05 standard:

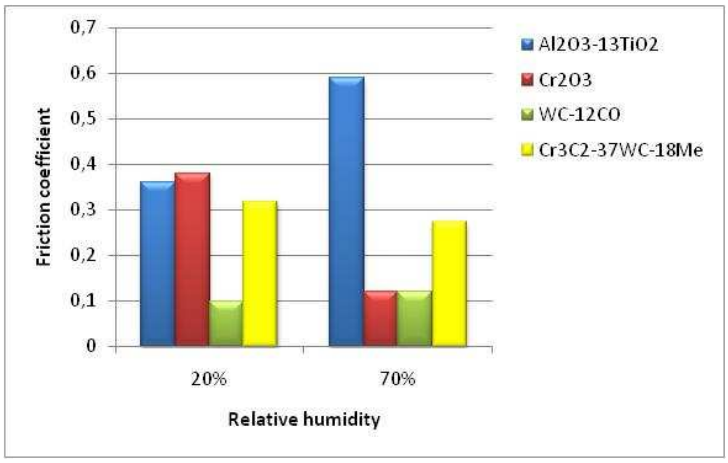

Figure 2 - Mean values of friction coefficient.

$$(1) \qquad V_{loss} = \frac{\pi r_u s^3}{6 r_p} \ [mm^3]$$

where:

r_u = wear track radius equal to 20 *mm*;

s = wear track thickness equal to 6 *mm*;

r_p = pin radius equal to 3 *mm*.

Wear rate is obtained dividing loss volume [mm^3] by the product of normal load applied [N] and sliding distance [m]. Mean values of the wear rate calculated at the end of the wear tests are reported in Figure 4.

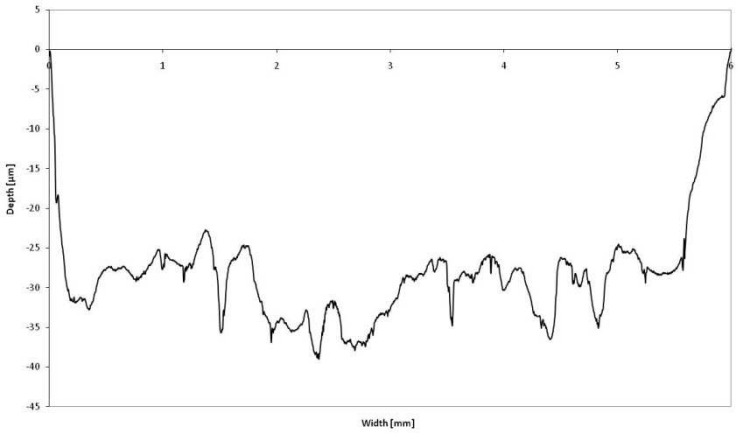

Figure 3 - Wear scar profile of the Al_2O_3-$13TiO_2$ coating after a wear test carried out under an applied normal load of 50 N and a relative humidity of 70%.

As can be seen, cermet coatings possess the highest wear resistance, typical of carbide-based coatings, with a wear rate in the range of 10^{-6} mm^3/Nm. The wear rates of plasma-spraying coatings at the two different humidity conditions are the highest, with the maximum values corresponding to the Al_2O_3-$13TiO_2$ coating.

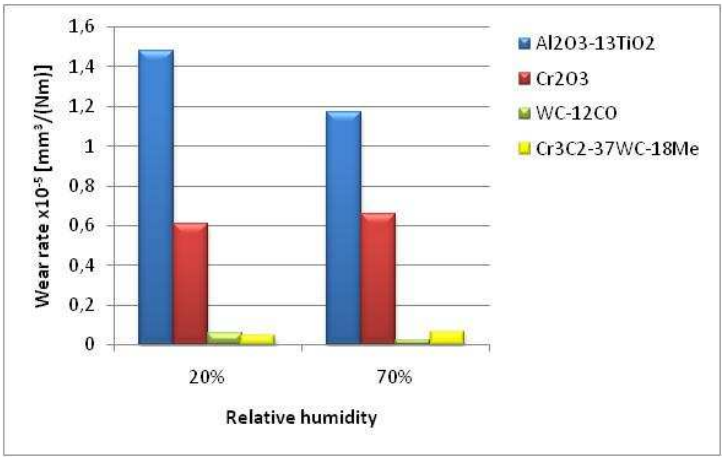

Figure 4 - Mean values of wear rate.

3.3 SEM analysis of worn surfaces

SEM micrographs in Figure 5 depict the Al_2O_3-$13TiO_2$ worn surfaces when the wear tests are performed under 20% and 70% relative humidity conditions. As can be noted, the worn surfaces are composed of smooth regions and rough regions. On the rough areas (Figure 5a) many microcracks and the removal of micro-sized sheet debris can be observed. It is also confirmed that the surface microfractures take place along the columnar grains and splat boundaries, since their strength is usually not high enough. The smooth areas (Figure 5b) are characterised, particularly in wet conditions, by the presence of small debris due to the removal of a thin aluminium hydroxide film, produced by tribochemical reactions between water vapour and the coating surface. The tribolayer is softer than the coating and is therefore able to reduce the wear damage, limiting the generation of surface microcracks [18-20].

SEM micrographs of Cr_2O_3 worn surfaces are shown in Figure 6. In both dry and wet conditions open pores and wear particles are visible; many cracks are also developed from the open porosity in perpendicular direction to the coating surface, generating interconnecting porosity (Figure 7).

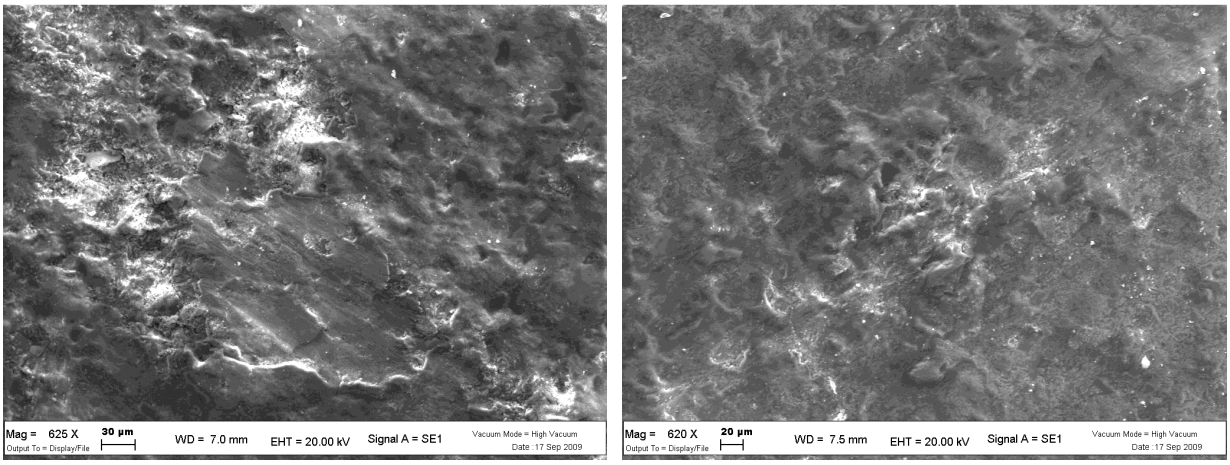

(a) (b)

Figure 5 - SEM micrographs of Al_2O_3-13TiO_2 worn surfaces, after the wear tests: (a) under a relative humidity of 20%, (b) under a relative humidity of 70%.

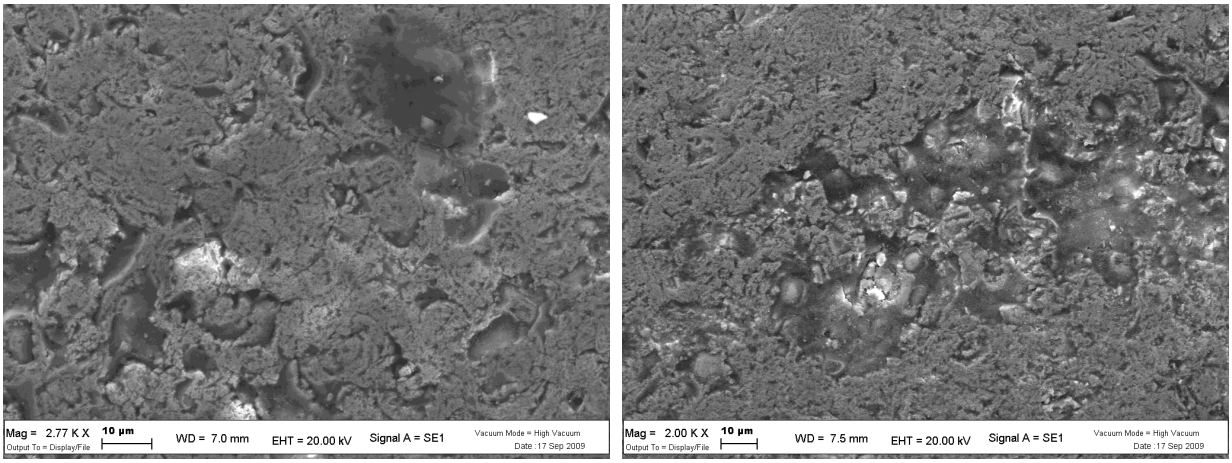

(a) (b)

Figure 6 - SEM micrographs of Cr_2O_3 worn surfaces, after the wear tests: (a) under a relative humidity of 20%, (b) under a relative humidity of 70%.

In Figure 7 are reported the SEM micrographs of WC-12Co worn surfaces. For this coating, the wear mechanism that can explain the low friction coefficient and the low wear rate is the formation of lubricant oxides, such as CoO and WO_3. At the beginning of the test the material loss mainly comes from the Co matrix removal. The removal of the metallic binder is followed by a decrease of the adhesion of WC particles, which are pull off giving as a result the formation of wear debris. The wear particles are subsequently flaked and oxidated, promoting the generation of lubricant oxides which are retained between the coupling surfaces [21, 22]. As the wear test prooceds the tribolayer is cracked and progressively removed (Figure 8a). In particular, for the highest value of relative humidity the tribolayers

appears more discontinuous, confirming that the presence of water vapour reduces the adhesion of the oxide film (Figure 8b).

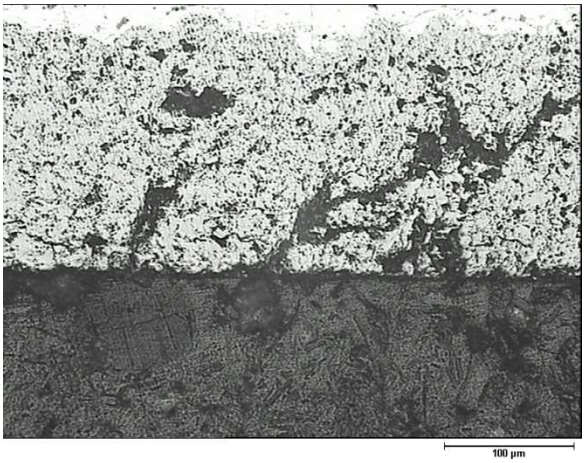

Figure 7 - Optical micrograph of Cr_2O_3 coatings' cross-section after a wear test carried out under a relative humidity of 70%.

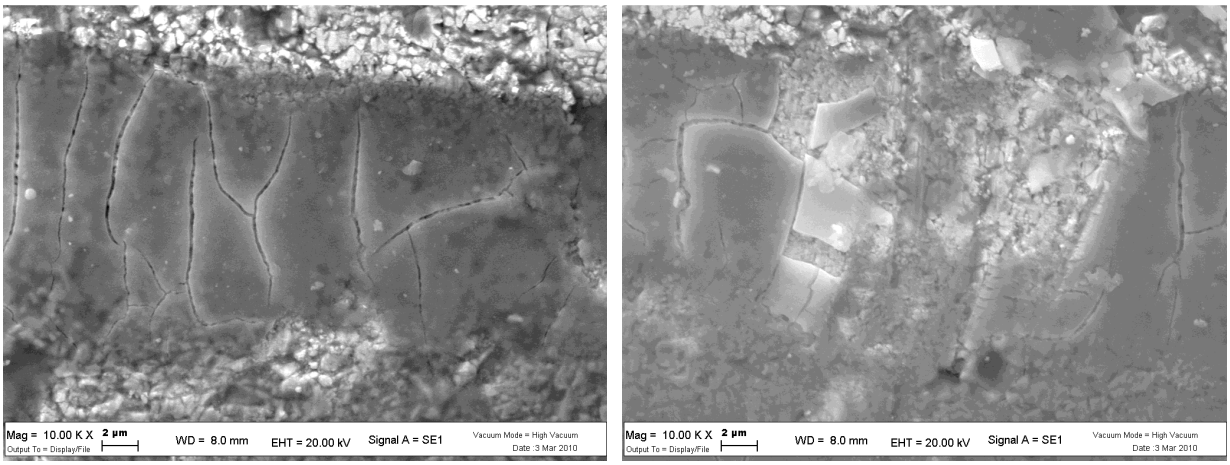

(a) (b)

Figure 8 - SEM micrographs of WC-12Co worn surfaces, after the wear tests: (a) under a relative humidity of 20%, (b) under a relative humidity of 70%.

Figure 9 shows a SEM micrograph of the Cr_3C_2-37WC-18Me worn surface, after a wear test carried out under a relative humidity of 70%. In any case, no wear damage is observed on this cermet coating. The Scanning Electron Microscope (SEM) observation is not clarifying of the wear mechanism that seems compatible with both the formation of a protective tribolayer and the plastic deformation of the asperities due to the high surface roughness that characterizes this coating. Further analyses by X-ray diffraction (XRD) could provide others information about the involved wear mechanisms.

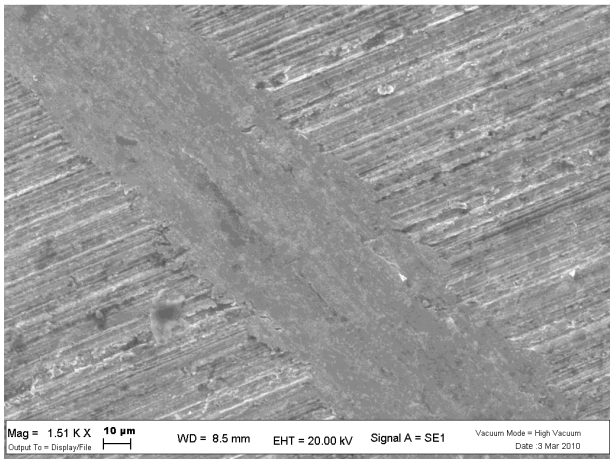

Figure 9 - SEM micrograph of Cr_3C_2-37WC-18Me coating after a wear test carried out under a relative humidity of 70%.

4. CONCLUSIONS

The analyses performed in this research activity demonstrate the importance of relative humidity on the tribological behaviour of ceramic and cermet coatings realised by means of plasma-spraying and HVOF-spraying techniques. In particular, the ceramic coatings (Al_2O_3-13TiO_2 and Cr_2O_3) are more sensitive to moisture than the cermet coatings (WC-12Co and Cr_3C_2-37WC-18Me), as highlighted by both the friction coefficient and wear rate results. Moreover, comparing the behaviour of the investigated coatings, the cermets ones present the best wear resistance. The SEM observations of the Al_2O_3-13TiO_2 worn surface show a non-protective tribolayer and the generation of surface microcracks with the consequent removal of wear debris in the form of flakes. The Cr_2O_3 worn surface appears smoother without evidence of significant wear and the pores remain open in the flattened surface. Many cracks are also propagated in the same direction as the normal load applied. WC-12Co coating is less sensitive to moisture due to the formation of oxide layers acting as a solid lubricant. Finally, the morphology of Cr_3C_2-37WC-18Me does not clarify the influence of relative humidity on the tribological behaviour of this coating.

ACKNOWLEDGEMENTS

The authors would like to thank Zocca Officine Meccaniche (Funo, BO) for the manufacturing of thermal-sprayed coating.

REFERENCES

1) J.E. FERNANDEZ et al., Friction and wear behaviour of plasma-sprayed Cr_2O_3 coatings against steel in a wide range of sliding velocities and normal loads, Tribology International 29-4, (1996), p. 333-343
2) M. HARJU et al., Influence of long-term aqueous exposure on surface properties of plasma sprayed oxides Al_2O_3, TiO_2 and their mixture Al_2O_3-13TiO_2, Applied Surface Science 254, (2008), p. 7272-7279
3) M. HARJU et al., Influence of aqueous aging on surface properties of plasma sprayed oxide coatings, Journal of Colloid and Interface Science 313, (2007), p. 194-201
4) D.A. STEWART, P.H. SHIPWAY, D.G. McCARTNEY, Microstructural evolution in thermally spayed WC-Co coatings: comparison between nanocomposite and conventional starting powders, Acta Materialia 48, (2000), p.1593-1604
5) H.S. AHN, O.K. KWON, Tribological behaviour of plasma-sprayed chromium oxide coating, Wear 225-229, (1999), p. 814-824
6) V. ARONOV, T. MESYEF, Wear in ceramic/ceramic and ceramic/metal reciprocating sliding contact: Part 1, Journal of Tribology 108, (1986), p. 16-21
7) G. BOLELLI et al., Wear behaviour of thermally sprayed ceramic oxide coatings, Wear 261, (2006), p. 1298-1315
8) J.M. GUILEMANY et al., Role of three-body abrasion wear in the sliding wear behaviour of WC-Co coatings obtained by thermal spraying, Surface and Coatings Technology 140, (2001), p. 141-146
9) A. SCRIVANI et al., A contribution to the surface analysis and characterization of HVOF coatings for petrochemical application, Wear 250, (2001), p. 107-113
10) P.H. SHIPWAY, L. HOWELL, Microscale abrasion-corrosion behaviour of WC-Co hardmetals and HVOF sprayed coatings, Wear 258, (2005), p. 303-312
11) J. VINCENZI et al., HVOF-coatings against high-temperature erosion (≈300°C) by cold fly ash in thermoelectric power plant, Materials & Design 27, (2006), p. 236-242
12) H. HERMAN, S. SAMPATH, R. McCUNE, Thermal spray: current status and future trends, in: S. SAMPATH, R. McCUNE (Eds), Thermal Spray Processing of Materials, MRS Bulletin, (2000), p. 17-25
13) Y. LIU, T.E. FISHER, A. DENT, Comparison of HVOF and plasma-sprayed alumina/titania coatings-microstructure, mechanical properties and abrasion behaviour, Surface and Coatings Technology 167, (2003), p. 68-76

14) R.S. LIMA, B.R. MARPLE, Optimized HVOF titania coatings, Journal of Thermal Spray Technology 12, (2003), p. 360-369

15) L. BIANCHI et al., Microstructural investigation of plasma-sprayed ceramic splats, Thin Solid Films 299, (1997), p. 125-135

16) J.K. LANCASTER, A review of the influence of environmental humidity and water on friction, lubrication and wear, Tribology International 23-6, (1990), p. 371-389

17) R.J.K. WOOD, Tribology of thermal sprayed WC-Co coatings, International Journal of Refractory Metals & Hard Materials 28, (2010), p. 82-94

18) X. DONG et al., Tribological characteristics of α-alumina at elevated temperatures, Journal of the American Ceramic Society 74, (1991), p. 1036-1044

19) W. TIAN et al., Sliding wear and electrochemical corrosion behaviour of plasma sprayed nanocomposite Al_2O_3-13TiO_2 coatings, Materials Chemistry and Physics 118, (2009), p. 37-45

20) B. NORMAND et al., Tribological properties of plasma sprayed alumina-titania coatings: role and control of the microstructure, Surface and Coatings Technology 123, (2000), p. 278-287

21) M. MAGNANI et al., Influence of HVOF parameters on the corrosion and wear resistance of WC-Co coatings sprayed on AA7050 T7, Surface & Coatings Technology 202, (2008), p. 4746-4757

22) P.H. SHIPWAY et al., Sliding wear behaviour of conventional and nanostructured HVOF sprayed WC-Co coatings, Wear 259, (2005), p. 820-827